Low cost a posteriori error estimators for an augmented mixed FEM in linear elasticity

Tomás P. Barrios[a], Edwin M. Behrens[b], María González[c]

[a] *Departamento de Matemática y Física Aplicadas, Universidad Católica de la Santísima Concepción, Concepción (Chile). E-mail:* tomas@ucsc.cl
[b] *Departamento de Ingeniería Civil, Universidad Católica de la Santísima Concepción, Concepción (Chile). E-mail:* ebehrens@ucsc.cl
[c] *Departamento de Matemáticas, Universidade da Coruña, Campus de Elviña s/n, 15071, A Coruña (Spain). E-mail:* maria.gonzalez.taboada@udc.es *and Basque Center for Applied Mathematics, C/Alameda de Mazarredo 14, 48009, Bilbao (Spain).*

Abstract

We consider an augmented mixed finite element method applied to the linear elasticity problem and derive a posteriori error estimators that are simpler and easier to implement than the ones available in the literature. In the case of homogeneous Dirichlet boundary conditions, the new a posteriori error estimator is reliable and locally efficient, whereas for non-homogeneous Dirichlet boundary conditions, we derive an a posteriori error estimator that is reliable and satisfies a *quasi-efficiency* bound. Numerical experiments illustrate the performance of the corresponding adaptive algorithms and support the theoretical results.

Key words: Linear elasticity, mixed finite element method, stabilization, a posteriori error estimates.
2000 MSC: 65N15, 65N30, 65N50, 74B05, 74S05

1. Introduction

In this paper, we consider the augmented dual-mixed method introduced in [11, 12] for the linear elasticity problem in the plane with Dirichlet boundary conditions and extended in [13] to the three-dimensional case. The approach in [11]-[13] relies on the mixed method of Hellinger and Reissner, that provides simultaneous approximations of the displacement $\mathbf{u}$ and the stress tensor $\boldsymbol{\sigma}$. The symmetry of $\boldsymbol{\sigma}$ is imposed weakly, through the

use of a Lagrange multiplier that can be interpreted as the rotation $\boldsymbol{\gamma} := \frac{1}{2}(\nabla \mathbf{u} - (\nabla \mathbf{u})^{\mathtt{t}})$. Then, suitable Galerkin least-squares type terms arising from the constitutive and equilibrium equations, and from the relation that defines the rotation in terms of the displacement are added. Besides, in the case of non-homogeneous Dirichlet boundary conditions, the bilinear form is augmented with a consistency term related with the boundary condition. The resulting augmented variational formulation is coercive in the whole space for appropriate values of the stabilization parameters, with a coercivity constant independent of the Lamé parameter λ. Therefore, the associated Galerkin scheme is well-posed and free of locking for *any* choice of finite element subspaces, which is in turn the main advantage of this method.

On the other hand, the use of adaptive algorithms based on a posteriori error estimates guarantees good convergence behavior of the finite element solution of a boundary value problem. Several a posteriori error estimators are already available in the literature for the usual mixed finite element method in linear elasticity (see [5, 8, 17, 9, 15, 7]). Concerning the a posteriori error analysis of the augmented scheme presented in [11] in the case of pure homogeneous Dirichlet boundary conditions, an a posteriori error estimator of residual type was introduced in [3]. That analysis was extended recently to the cases of pure non-homogeneous Dirichlet boundary conditions and mixed boundary conditions with non-homogeneous Neumann data; cf. [4]. The a posteriori error estimators derived in [3] and [4] are both reliable and efficient, and involve the computation of eleven residuals per element in the homogeneous case, and thirteen residuals per element in the non-homogeneous one; both include normal and tangential jumps.

In this paper, we present new a posteriori error estimators for the augmented dual-mixed methods proposed in [11]-[13] in the case of Dirichlet boundary conditions. The analysis is based on the use of a projection of the error and the homogeneous and non-homogeneous cases are studied separately. In the case of homogeneous boundary conditions, we obtain an a posteriori error estimator that is reliable, locally efficient and only requires the computation of four residuals per element. Moreover, this a posteriori error estimator is the first one derived for the augmented method proposed in [13]. When non-homogeneous boundary conditions are imposed, we derive two new reliable a posteriori error estimators, one valid in 2D and 3D, and a second one that is only valid in 2D. The latter is locally efficient in the elements that do not touch the boundary and requires the computation of four residuals per element in the interior triangles, five residuals per element

in the triangles with exactly one node on the boundary and six residuals per element in the triangles with a side on the boundary. Neither of these a posteriori error estimators require the computation of normal nor tangential jumps, which makes them easy to implement.

The rest of the paper is organized as follows. In Section 2 we recall the main features of the augmented dual-mixed method introduced in [11, 13] for the linear elasticity problem with homogeneous Dirichlet boundary conditions. Then, we use the Ritz projection of the error to derive the new a posteriori error estimator and show that it is reliable and locally efficient. The extension to the case of non-homogeneous Dirichlet boundary conditions is developed in Section 3, where we first recall the dual-mixed method from [12, 13]. Finally, in Section 4 we provide several numerical experiments that illustrate the performance of the corresponding adaptive algorithms and support the theoretical results.

In what follows, we will use the standard notations for Sobolev spaces and norms. We let $\Omega \subset \mathbb{R}^d$ $(d = 2, 3)$ be a bounded domain with a Lipschitz-continuous boundary Γ. We denote $H(\mathbf{div}; \Omega) := \{\boldsymbol{\tau} \in [L^2(\Omega)]^{d\times d} : \mathbf{div}(\boldsymbol{\tau}) \in [L^2(\Omega)]^d\}$, $H_0 := \{\boldsymbol{\tau} \in H(\mathbf{div}; \Omega) : \int_\Omega \mathrm{tr}(\boldsymbol{\tau}) = 0\}$ and $[L^2(\Omega)]^{d\times d}_{\mathtt{skew}} := \{\boldsymbol{\eta} \in [L^2(\Omega)]^{d\times d} : \boldsymbol{\eta} + \boldsymbol{\eta}^{\mathtt{t}} = \mathbf{0}\}$. The duality pairing between $[H^{-1/2}(\Gamma)]^d$ and $[H^{1/2}(\Gamma)]^d$ with respect to the $[L^2(\Gamma)]^d$-inner product is denoted by $\langle\cdot,\cdot\rangle_\Gamma$. Finally, we use C or c, with or without subscripts, to denote generic constants, independent of the discretization parameter, that may take different values at different occurrences.

2. Homogeneous Dirichlet boundary conditions

Let $\mathbf{f} \in [L^2(\Omega)]^d$ be a given volume force. We denote by $\mathcal{C}$ the elasticity operator determined by Hooke's law, that is,

$$\mathcal{C}\,\boldsymbol{\zeta} \;:=\; \lambda\,\mathrm{tr}(\boldsymbol{\zeta})\,\mathbf{I} \;+\; 2\,\mu\,\boldsymbol{\zeta}\,, \qquad \forall\,\boldsymbol{\zeta} \,\in\, [L^2(\Omega)]^{d\times d}\,, \tag{1}$$

where λ, $\mu > 0$ are the Lamé parameters and $\mathbf{I}$ is the identity matrix in $\mathbb{R}^{d\times d}$. The problem of linear elasticity with homogeneous Dirichlet boundary conditions consists in finding the displacement $\mathbf{u}$ and the stress tensor $\boldsymbol{\sigma}$ such that

$$\left\{\begin{array}{rcll} -\mathbf{div}(\boldsymbol{\sigma}) & = & \mathbf{f} & \text{in} \quad \Omega, \\ \boldsymbol{\sigma} & = & \mathcal{C}\,\boldsymbol{\varepsilon}(\mathbf{u}) & \text{in} \quad \Omega, \\ \mathbf{u} & = & \mathbf{0} & \text{on } \Gamma, \end{array}\right. \tag{2}$$

where $\boldsymbol{\varepsilon}(\mathbf{u}) := \frac{1}{2}\,(\nabla\mathbf{u} + (\nabla\mathbf{u})^{\mathtt{t}})$ is the strain tensor of small deformations. In the next subsection, we recall the augmented dual-mixed method proposed in [11, 13] to solve problem (2).

2.1. The augmented dual-mixed finite element method

Let κ_1, κ_2 and κ_3 be positive parameters. We denote $\mathbf{H} := H_0 \times [H^1_0(\Omega)]^d \times [L^2(\Omega)]^{d\times d}_{\mathtt{skew}}$ and $\tilde{\mathbf{H}} := H_0 \times [H^1(\Omega)]^d \times [L^2(\Omega)]^{d\times d}_{\mathtt{skew}}$. We define the bilinear form $A : \tilde{\mathbf{H}} \times \tilde{\mathbf{H}} \to \mathbb{R}$ and the linear functional $F : \tilde{\mathbf{H}} \to \mathbb{R}$ as follows:

$$\begin{aligned} A((\boldsymbol{\sigma},\mathbf{u},\boldsymbol{\gamma}),(\boldsymbol{\tau},\mathbf{v},\boldsymbol{\eta})) &:= \int_\Omega \mathcal{C}^{-1}\boldsymbol{\sigma} : \boldsymbol{\tau} \,+\, \int_\Omega \mathbf{u}\cdot\mathbf{div}(\boldsymbol{\tau}) \,+\, \int_\Omega \boldsymbol{\tau} : \boldsymbol{\gamma} \\ &- \int_\Omega \mathbf{v}\cdot\mathbf{div}(\boldsymbol{\sigma}) \,-\, \int_\Omega \boldsymbol{\sigma} : \boldsymbol{\eta} \,+\kappa_1 \int_\Omega \big(\boldsymbol{\varepsilon}(\mathbf{u}) - \mathcal{C}^{-1}\boldsymbol{\sigma}\big) : \big(\boldsymbol{\varepsilon}(\mathbf{v}) + \mathcal{C}^{-1}\boldsymbol{\tau}\big) \\ &+\kappa_3 \int_\Omega \left(\boldsymbol{\gamma} - \frac{1}{2}(\nabla\mathbf{u} - (\nabla\mathbf{u})^{\mathtt{t}})\right) : \left(\boldsymbol{\eta} + \frac{1}{2}(\nabla\mathbf{v} - (\nabla\mathbf{v})^{\mathtt{t}})\right) \\ &+\kappa_2 \int_\Omega \mathbf{div}(\boldsymbol{\sigma})\cdot\mathbf{div}(\boldsymbol{\tau})\,, \qquad \forall\,(\boldsymbol{\sigma},\mathbf{u},\boldsymbol{\gamma}),(\boldsymbol{\tau},\mathbf{v},\boldsymbol{\eta}) \in \tilde{\mathbf{H}}\,, \end{aligned} \tag{3}$$

and

$$F(\boldsymbol{\tau},\mathbf{v},\boldsymbol{\eta}) \,:=\, \int_\Omega \mathbf{f}\cdot(\,\mathbf{v} \,-\, \kappa_2\,\mathbf{div}(\boldsymbol{\tau})\,)\,, \qquad \forall\,(\boldsymbol{\tau},\mathbf{v},\boldsymbol{\eta}) \in \tilde{\mathbf{H}}\,, \tag{4}$$

where $\mathcal{C}^{-1}\,\boldsymbol{\zeta} := \frac{1}{2\,\mu}\,\boldsymbol{\zeta} \,-\, \frac{\lambda}{2\,\mu\,(d\,\lambda+2\,\mu)}\,\mathrm{tr}(\boldsymbol{\zeta})\,\mathbf{I}$, $\forall\,\boldsymbol{\zeta} \,\in\, [L^2(\Omega)]^{d\times d}$.

The augmented variational formulation proposed in [11, 13] reads: find $(\boldsymbol{\sigma},\mathbf{u},\boldsymbol{\gamma}) \,\in\, \mathbf{H}$ such that

$$A((\boldsymbol{\sigma},\mathbf{u},\boldsymbol{\gamma}),(\boldsymbol{\tau},\mathbf{v},\boldsymbol{\eta})) = F(\boldsymbol{\tau},\mathbf{v},\boldsymbol{\eta})\,, \qquad \forall\,(\boldsymbol{\tau},\mathbf{v},\boldsymbol{\eta}) \,\in\, \mathbf{H}\,. \tag{5}$$

From now on, we assume that the parameters κ_1, κ_2 and κ_3 are chosen independently of λ and such that $\kappa_1 \,\in\, (0, 2\,\mu)$, $\kappa_2 \,>\, 0$ and $\kappa_3 \,\in\, (0, \kappa_1)$. Under these assumptions (cf. Theorem 3.1 in [11] and Theorem 5.1 in [13]), there exist positive constants, M and α, independent of λ, such that for all $(\boldsymbol{\sigma},\mathbf{u},\boldsymbol{\gamma})$, $(\boldsymbol{\tau},\mathbf{v},\boldsymbol{\eta}) \in \mathbf{H}$ we have

$$|A((\boldsymbol{\sigma},\mathbf{u},\boldsymbol{\gamma}),(\boldsymbol{\tau},\mathbf{v},\boldsymbol{\eta}))| \;\leq\; M\,\|(\boldsymbol{\sigma},\mathbf{u},\boldsymbol{\gamma})\|_{\mathbf{H}}\;\|(\boldsymbol{\tau},\mathbf{v},\boldsymbol{\eta})\|_{\mathbf{H}}\,,$$

$$A((\boldsymbol{\tau},\mathbf{v},\boldsymbol{\eta}),(\boldsymbol{\tau},\mathbf{v},\boldsymbol{\eta})) \;\geq\; \alpha\;\|(\boldsymbol{\tau},\mathbf{v},\boldsymbol{\eta})\|^2_{\mathbf{H}}\,,$$

where $\|\cdot\|_{\mathbf{H}}$ denotes the product norm of $\mathbf{H}$:

$$\|(\boldsymbol{\tau},\mathbf{v},\boldsymbol{\eta})\|^2_{\mathbf{H}} := \|\boldsymbol{\tau}\|^2_{H(\mathbf{div},\Omega)} + \|\mathbf{v}\|^2_{[H^1(\Omega)]^d} + \|\boldsymbol{\eta}\|^2_{[L^2(\Omega)]^{d\times d}}, \quad \forall\,(\boldsymbol{\tau},\mathbf{v},\boldsymbol{\eta}) \in \mathbf{H}.$$

As a consequence (cf. [11, Theorem 3.2] and Section 5 in [13]), the augmented variational formulation (5) has a unique solution $(\boldsymbol{\sigma},\mathbf{u},\boldsymbol{\gamma}) \in \mathbf{H}$ and there exists a positive constant C, independent of λ, such that

$$\|(\boldsymbol{\sigma},\mathbf{u},\boldsymbol{\gamma})\|_{\mathbf{H}} \,\leq\, C\,\|\mathbf{f}\|_{[L^2(\Omega)]^d}\,.$$

Now, let h be a positive parameter and consider a finite dimensional subspace $\mathbf{H}_h \subset \mathbf{H}$. The Galerkin scheme associated to problem (5) reads: find $(\boldsymbol{\sigma}_h,\mathbf{u}_h,\boldsymbol{\gamma}_h) \in \mathbf{H}_h$ such that

$$A((\boldsymbol{\sigma}_h,\mathbf{u}_h,\boldsymbol{\gamma}_h),(\boldsymbol{\tau}_h,\mathbf{v}_h,\boldsymbol{\eta}_h)) \,=\, F(\boldsymbol{\tau}_h,\mathbf{v}_h,\boldsymbol{\eta}_h)\,, \quad \forall\,(\boldsymbol{\tau}_h,\mathbf{v}_h,\boldsymbol{\eta}_h) \in \mathbf{H}_h\,. \quad (6)$$

The existence and uniqueness of a solution to problem (6) as well as a Céa estimate are established in Theorem 4.1 in [11] and Section 5 in [13] under the assumptions made before on $\bar{\kappa}$.

In order to describe the choice of finite element subspaces for the Galerkin scheme (6) that requires less degrees of freedom (dof), we assume now that Ω is a polygonal (if $d=2$) or polyhedral (if $d=3$) region and let $\{\mathcal{T}_h\}_{h>0}$ be a regular family of meshes of $\bar{\Omega}$, made up of triangles in 2D or tetrahedra in 3D, such that $\bar{\Omega} = \cup\{\,T : T\in\mathcal{T}_h\,\}$. Given an element $T\in\mathcal{T}_h$, we denote by h_T its diameter and define the mesh size $h := \max\{\,h_T : T\in\mathcal{T}_h\,\}$. In addition, given an integer $\ell\geq 0$ and a subset S of $\mathbb{R}^d$, we denote by $\mathcal{P}_\ell(S)$ the space of polynomials in d variables defined in S of total degree at most ℓ, and for each $T\in\mathcal{T}_h$, we define the local Raviart-Thomas space of the lowest order, $\mathcal{RT}_0(T) := \langle\,\mathbf{e}_1,\ldots,\mathbf{e}_d,\mathbf{x}\,\rangle \subseteq [\mathcal{P}_1(T)]^d$, where $\{\mathbf{e}_i\}_{i=1}^d$ is the canonical basis of $\mathbb{R}^d$ and $\mathbf{x}$ is a generic vector of $\mathbb{R}^d$. Then, we define the finite element subspaces

$$H_h^{\boldsymbol{\sigma}} := \left\{\boldsymbol{\tau}_h\in H(\mathbf{div};\Omega) : \boldsymbol{\tau}_h|_T \in [\mathcal{RT}_0(T)^{\mathtt{t}}]^d,\ \forall\,T\in\mathcal{T}_h;\ \int_\Omega \mathrm{tr}(\boldsymbol{\tau}_h) = 0\right\}, \quad (7)$$

$$H_h^{\mathbf{u}} := \left\{\,\mathbf{v}_h \in [\mathcal{C}(\bar{\Omega})\cap H^1_0(\Omega)]^d : \mathbf{v}_h|_T \in [\mathcal{P}_1(T)]^d\,, \quad \forall\,T\in\mathcal{T}_h\,\right\},$$

$$H_h^{\boldsymbol{\gamma}} := \left\{\,\boldsymbol{\eta}_h \in [L^2(\Omega)]^{d\times d}_{\mathtt{skew}} : \boldsymbol{\eta}_h|_T \in [\mathcal{P}_0(T)]^{d\times d}, \quad \forall\,T\in\mathcal{T}_h\,\right\}. \quad (8)$$

The simplest choice of finite element subspaces for the Galerkin scheme (6) is $\mathbf{H}_h := H_h^{\boldsymbol{\sigma}}\times H_h^{\mathbf{u}}\times H_h^{\boldsymbol{\gamma}}$. In this special case, if the solution to problem

(5) is sufficiently smooth, we can expect the following rate of convergence (cf. [11, 13]):

$$\begin{aligned}\|(\boldsymbol{\sigma},\mathbf{u},\boldsymbol{\gamma})-(\boldsymbol{\sigma}_h,\mathbf{u}_h,\boldsymbol{\gamma}_h)\|_{\mathbf{H}} \leq C\,h^r\,\Big(\,\|\boldsymbol{\sigma}\|_{[H^r(\Omega)]^{d\times d}} \\ +\|\mathbf{div}(\boldsymbol{\sigma})\|_{[H^r(\Omega)]^d}+\|\mathbf{u}\|_{[H^{r+1}(\Omega)]^d}+\|\boldsymbol{\gamma}\|_{[H^r(\Omega)]^{d\times d}}\,\Big)\,,\end{aligned} \tag{9}$$

where $r\in(0,1]$ and $C>0$ is a constant independent of h and λ.

Let m be the number of elements in $\mathcal{T}_h$. For the previous choice of finite element subspaces, the total number of dof when $d=2$ behaves asymptotically as $5\,m$, whereas for PEERS and BDM (after a static condensation process), it behaves asymptotically as $7.5\,m$ and $9\,m$, respectively. In 3D, the total number of dof behaves approximately as $9.5\,m$, whereas for the classical PEERS in 3D the total number of dof behaves approximately as $12.5\,m$ (both methods accept a reduction of 3 local dof using static condensation). For a comparison with the mixed finite element methods derived using finite element exterior calculus, see [4, 13].

2.2. A posteriori error analysis

In this section, we develop an a posteriori error analysis for the discrete scheme (6) based on the use of an appropriate projection of the error. Up to the authors' knowlegde, this idea was first used in [2] to derive an a posteriori error estimator for an augmented dual-mixed method for the Poisson equation.

Throughout this section, we assume that the stabilization parameters are such that problems (5) and (6) are well-posed. Let $(\boldsymbol{\sigma},\mathbf{u},\boldsymbol{\gamma})$ and $(\boldsymbol{\sigma}_h,\mathbf{u}_h,\boldsymbol{\gamma}_h)$ be the unique solutions to problems (5) and (6), respectively. We define the Ritz projection of the error, $(\bar{\boldsymbol{\sigma}},\bar{\mathbf{u}},\bar{\boldsymbol{\gamma}})$, as the unique element in $\mathbf{H}$ such that

$$\langle(\bar{\boldsymbol{\sigma}},\bar{\mathbf{u}},\bar{\boldsymbol{\gamma}}),(\boldsymbol{\tau},\mathbf{v},\boldsymbol{\eta})\rangle_{\mathbf{H}} = A((\boldsymbol{\sigma}-\boldsymbol{\sigma}_h,\mathbf{u}-\mathbf{u}_h,\boldsymbol{\gamma}-\boldsymbol{\gamma}_h),(\boldsymbol{\tau},\mathbf{v},\boldsymbol{\eta}))\,, \tag{10}$$

for all $(\boldsymbol{\tau},\mathbf{v},\boldsymbol{\eta})\in\mathbf{H}$, where

$$\langle(\boldsymbol{\zeta},\mathbf{w},\boldsymbol{\rho}),(\boldsymbol{\tau},\mathbf{v},\boldsymbol{\eta})\rangle_{\mathbf{H}} := (\boldsymbol{\zeta},\boldsymbol{\tau})_{H(\mathbf{div};\Omega)}+(\mathbf{w},\mathbf{v})_{[H^1(\Omega)]^d}+(\boldsymbol{\rho},\boldsymbol{\eta})_{[L^2(\Omega)]^{d\times d}}\,,$$

for any $(\boldsymbol{\zeta},\mathbf{w},\boldsymbol{\rho})$, $(\boldsymbol{\tau},\mathbf{v},\boldsymbol{\eta})\in\mathbf{H}$. We remark that the existence and uniqueness of $(\bar{\boldsymbol{\sigma}},\bar{\mathbf{u}},\bar{\boldsymbol{\gamma}})$ is guaranteed by the Lax-Milgram Lemma.

Now, using the coercivity of the bilinear form $A(\cdot,\cdot)$, we easily get that

$$||(\boldsymbol{\sigma}-\boldsymbol{\sigma}_h,\mathbf{u}-\mathbf{u}_h,\boldsymbol{\gamma}-\boldsymbol{\gamma}_h)||_{\mathbf{H}} \leq \frac{1}{\alpha}\,||(\bar{\boldsymbol{\sigma}},\bar{\mathbf{u}},\bar{\boldsymbol{\gamma}})||_{\mathbf{H}}\,. \tag{11}$$

Hence, to obtain reliable a posteriori error estimates for the discrete scheme (6), it is enough to bound from above the Ritz projection of the error. In the next Lemma we obtain such an upper bound.

Lemma 1. *There exists a constant $C > 0$, independent of h and λ, such that*

$$||(\bar{\boldsymbol{\sigma}}, \bar{\mathbf{u}}, \bar{\boldsymbol{\gamma}})||_{\mathbf{H}} \leq C \Big(||\mathbf{f} + \mathbf{div}(\boldsymbol{\sigma}_h)||_{[L^2(\Omega)]^d} + ||\boldsymbol{\sigma}_h - \boldsymbol{\sigma}_h^{\mathtt{t}}||_{[L^2(\Omega)]^{d\times d}} + ||\boldsymbol{\varepsilon}(\mathbf{u}_h) - \mathcal{C}^{-1}\boldsymbol{\sigma}_h||_{[L^2(\Omega)]^{d\times d}} + \big|\big|\boldsymbol{\gamma}_h - \tfrac{1}{2}(\nabla \mathbf{u}_h - (\nabla \mathbf{u}_h)^{\mathtt{t}})\big|\big|_{[L^2(\Omega)]^{d\times d}} \Big).$$

Proof. Taking into account that $(\boldsymbol{\sigma}, \mathbf{u}, \boldsymbol{\gamma})$ is the solution to problem (5), we deduce from (10) that

$$\langle (\bar{\boldsymbol{\sigma}}, \bar{\mathbf{u}}, \bar{\boldsymbol{\gamma}}), (\boldsymbol{\tau}, \mathbf{v}, \boldsymbol{\eta}) \rangle_{\mathbf{H}} = F(\boldsymbol{\tau}, \mathbf{v}, \boldsymbol{\eta}) - A((\boldsymbol{\sigma}_h, \mathbf{u}_h, \boldsymbol{\gamma}_h), (\boldsymbol{\tau}, \mathbf{v}, \boldsymbol{\eta})), \qquad (12)$$

for any $(\boldsymbol{\tau}, \mathbf{v}, \boldsymbol{\eta}) \in \mathbf{H}$. Then, using the definitions of the linear functional F and the bilinear form $A(\cdot, \cdot)$, equation (12) can be written equivalently as follows

$$\begin{cases} (\bar{\boldsymbol{\sigma}}, \boldsymbol{\tau})_{H(\mathbf{div};\Omega)} = F_1(\boldsymbol{\tau}), & \forall\, \boldsymbol{\tau} \in H_0\,, \\ (\bar{\mathbf{u}}, \mathbf{v})_{[H^1(\Omega)]^d} = F_2(\mathbf{v}), & \forall\, \mathbf{v} \in [H_0^1(\Omega)]^d\,, \\ (\bar{\boldsymbol{\gamma}}, \boldsymbol{\eta})_{[L^2(\Omega)]^{d\times d}} = F_3(\boldsymbol{\eta}), & \forall\, \boldsymbol{\eta} \in [L^2(\Omega)]^{d\times d}_{\mathtt{skew}}\,, \end{cases}$$

where the bounded linear functionals F_1, F_2 and F_3 are defined by

$$\begin{aligned} F_1(\boldsymbol{\tau}) &:= -\kappa_2 \int_\Omega (\mathbf{f} + \mathbf{div}(\boldsymbol{\sigma}_h)) \cdot \mathbf{div}(\boldsymbol{\tau}) - \int_\Omega (\mathcal{C}^{-1}\boldsymbol{\sigma}_h + \boldsymbol{\gamma}_h) : \boldsymbol{\tau} \\ &\quad - \int_\Omega \mathbf{u}_h \cdot \mathbf{div}(\boldsymbol{\tau}) - \kappa_1 \int_\Omega (\boldsymbol{\varepsilon}(\mathbf{u}_h) - \mathcal{C}^{-1}\boldsymbol{\sigma}_h) : \mathcal{C}^{-1}\boldsymbol{\tau}, \\ F_2(\mathbf{v}) &:= \int_\Omega (\mathbf{f} + \mathbf{div}(\boldsymbol{\sigma}_h)) \cdot \mathbf{v} - \kappa_1 \int_\Omega \big(\boldsymbol{\varepsilon}(\mathbf{u}_h) - \mathcal{C}^{-1}\boldsymbol{\sigma}_h\big) : \boldsymbol{\varepsilon}(\mathbf{v}) \\ &\quad - \kappa_3 \int_\Omega (\boldsymbol{\gamma}_h - \frac{\nabla \mathbf{u}_h - (\nabla \mathbf{u}_h)^{\mathtt{t}}}{2}) : \frac{\nabla \mathbf{v} - (\nabla \mathbf{v})^{\mathtt{t}}}{2}\,, \\ F_3(\boldsymbol{\eta}) &:= \int_\Omega \boldsymbol{\sigma}_h : \boldsymbol{\eta} - \kappa_3 \int_\Omega (\boldsymbol{\gamma}_h - \frac{\nabla \mathbf{u}_h - (\nabla \mathbf{u}_h)^{\mathtt{t}}}{2}) : \boldsymbol{\eta}\,. \end{aligned}$$

Integrating by parts in the third term in F_1, we can write

$$\begin{aligned} F_1(\boldsymbol{\tau}) &= -\kappa_2 \int_\Omega (\mathbf{f} + \mathbf{div}(\boldsymbol{\sigma}_h)) \cdot \mathbf{div}(\boldsymbol{\tau}) - \int_\Omega (\mathcal{C}^{-1}\boldsymbol{\sigma}_h - \nabla \mathbf{u}_h + \boldsymbol{\gamma}_h) : \boldsymbol{\tau} \\ &- \kappa_1 \int_\Omega \mathcal{C}^{-1}(\boldsymbol{\varepsilon}(\mathbf{u}_h) - \mathcal{C}^{-1}\boldsymbol{\sigma}_h) : \boldsymbol{\tau}\,. \end{aligned}$$

On the other hand, we remark that

$$\int_\Omega \boldsymbol{\tau} : \frac{\nabla \mathbf{v} \pm (\nabla \mathbf{v})^{\mathtt{t}}}{2} = \int_\Omega \frac{\boldsymbol{\tau} \pm \boldsymbol{\tau}^{\mathtt{t}}}{2} : \nabla \mathbf{v}\,, \quad \forall\, \boldsymbol{\tau} \in [L^2(\Omega)]^{d\times d}\,. \tag{13}$$

Hence,

$$\begin{aligned} F_2(\mathbf{v}) &= \int_\Omega (\mathbf{f} + \mathbf{div}(\boldsymbol{\sigma}_h)) \cdot \mathbf{v} - \kappa_1 \int_\Omega (\boldsymbol{\varepsilon}(\mathbf{u}_h) - \mathcal{C}^{-1}\,\boldsymbol{\sigma}_h) : \nabla \mathbf{v} \\ &- \kappa_3 \int_\Omega (\boldsymbol{\gamma}_h - \frac{\nabla \mathbf{u}_h - (\nabla \mathbf{u}_h)^{\mathtt{t}}}{2}) : \nabla \mathbf{v}\,. \end{aligned}$$

Finally, using that $\boldsymbol{\eta}$ is skew-symmetric,

$$F_3(\boldsymbol{\eta}) = \int_\Omega \frac{\boldsymbol{\sigma}_h - \boldsymbol{\sigma}_h^{\mathtt{t}}}{2} : \boldsymbol{\eta} - \kappa_3 \int_\Omega (\boldsymbol{\gamma}_h - \frac{\nabla \mathbf{u}_h - (\nabla \mathbf{u}_h)^{\mathtt{t}}}{2}) : \boldsymbol{\eta}\,.$$

Then, the result follows using the Cauchy-Schwarz inequality, the continuity of $\mathcal{C}^{-1}$ and noting that

$$\begin{aligned} ||\mathcal{C}^{-1}\boldsymbol{\sigma}_h - \nabla \mathbf{u}_h + \boldsymbol{\gamma}_h||_{[L^2(\Omega)]^{d\times d}} &\leq ||\mathcal{C}^{-1}\boldsymbol{\sigma}_h - \boldsymbol{\varepsilon}(\mathbf{u}_h)||_{[L^2(\Omega)]^{d\times d}} \\ &+ \left|\left|\boldsymbol{\gamma}_h - \frac{\nabla \mathbf{u}_h - (\nabla \mathbf{u}_h)^{\mathtt{t}}}{2}\right|\right|_{[L^2(\Omega)]^{d\times d}}. \end{aligned}$$

□

Remark 2. *The constant C in Lemma 1 can be chosen as*

$$C = \max\,(1 + \kappa_2, 1 + \kappa_1\,(1 + \left|\left|\mathcal{C}^{-1}\right|\right|), 1 + 2\,\kappa_3),$$

where $||\mathcal{C}^{-1}|| := ||\mathcal{C}^{-1}||_{\mathcal{L}([L^2(\Omega)]^{d\times d},[L^2(\Omega)]^{d\times d})} \leq \frac{1}{2\,\mu}(1 + \frac{d\,\lambda}{d\,\lambda + 2\,\mu}) \leq \frac{1}{\mu}$.

Motivated by (11) and the bound obtained in Lemma 1, we define the a posteriori error estimator $\theta := \left(\sum_{T \in \mathcal{T}_h} \theta_T^2 \right)^{1/2}$, where

$$\theta_T^2 := ||\mathbf{f} + \mathbf{div}(\boldsymbol{\sigma}_h)||^2_{[L^2(T)]^d} + ||\boldsymbol{\sigma}_h - \boldsymbol{\sigma}_h^{\mathtt{t}}||^2_{[L^2(T)]^{d\times d}}$$
$$+ ||\boldsymbol{\varepsilon}(\mathbf{u}_h) - \mathcal{C}^{-1}\boldsymbol{\sigma}_h||^2_{[L^2(T)]^{d\times d}} + \left|\left|\boldsymbol{\gamma}_h - \frac{\nabla \mathbf{u}_h - (\nabla \mathbf{u}_h)^{\mathtt{t}}}{2}\right|\right|^2_{[L^2(T)]^{d\times d}}.$$

In the next Lemma we prove that θ is locally efficient.

Lemma 3. *There exists a positive constant $C_{\mathtt{eff}}$, independent of h and λ, such that*

$$\theta_T \leq C_{\mathtt{eff}}^{-1} \, ||(\boldsymbol{\sigma} - \boldsymbol{\sigma}_h, \mathbf{u} - \mathbf{u}_h, \boldsymbol{\gamma} - \boldsymbol{\gamma}_h)||_{\mathbf{H}(T)},$$

where $||\cdot||_{\mathbf{H}(T)}$ denotes the product norm of $\mathbf{H}(T) := H(\mathbf{div}; T) \times [H^1(T)]^d \times [L^2(T)]^{d\times d}$.

Proof. Using the equilibrium equation, the symmetry of $\boldsymbol{\sigma}$, the definition of $\boldsymbol{\gamma}$ in terms of the displacement and the triangle inequality, we easily get

$$||\mathbf{f} + \mathbf{div}(\boldsymbol{\sigma}_h)||^2_{[L^2(T)]^d} = ||\mathbf{div}(\boldsymbol{\sigma}_h - \boldsymbol{\sigma})||^2_{[L^2(T)]^d}, \tag{14}$$

$$||\boldsymbol{\sigma}_h - \boldsymbol{\sigma}_h^{\mathtt{t}}||^2_{[L^2(T)]^{d\times d}} \leq 4 \, ||\boldsymbol{\sigma}_h - \boldsymbol{\sigma}||^2_{[L^2(T)]^{d\times d}}, \tag{15}$$

$$\left|\left|\boldsymbol{\gamma}_h - \frac{\nabla \mathbf{u}_h - (\nabla \mathbf{u}_h)^{\mathtt{t}}}{2}\right|\right|^2_{[L^2(T)]^{d\times d}} \leq 2 \left(||\boldsymbol{\gamma} - \boldsymbol{\gamma}_h||^2_{[L^2(T)]^{d\times d}} + |\mathbf{u} - \mathbf{u}_h|^2_{[H^1(T)]^d} \right). \tag{16}$$

On the other hand, using the constitutive law, the triangle inequality and the continuity of $\mathcal{C}^{-1}$, we obtain that

$$\left|\left|\boldsymbol{\varepsilon}(\mathbf{u}_h) - \mathcal{C}^{-1}\boldsymbol{\sigma}_h\right|\right|^2_{[L^2(T)]^{d\times d}} \leq 2 \left(|\mathbf{u} - \mathbf{u}_h|^2_{[H^1(T)]^d} + \left|\left|\mathcal{C}^{-1}\right|\right| \, ||\boldsymbol{\sigma} - \boldsymbol{\sigma}_h||^2_{[L^2(T)]^{d\times d}} \right). \tag{17}$$

Then, the result follows from inequalities (14)-(17). □

Next we prove that θ is both reliable and efficient.

Theorem 4. *There exist positive constants, $C_{\mathtt{eff}}$ and $C_{\mathtt{rel}}$, independent of h and λ, such that*

$$C_{\mathtt{eff}} \, \theta \leq ||(\boldsymbol{\sigma} - \boldsymbol{\sigma}_h, \mathbf{u} - \mathbf{u}_h, \boldsymbol{\gamma} - \boldsymbol{\gamma}_h)||_{\mathbf{H}} \leq C_{\mathtt{rel}} \, \theta.$$

Proof. The reliability estimate follows from (11), Lemma 1 and the definition of θ. The efficiency follows from Lemma 3. $\square$

It is not difficult to see that $C_{\mathtt{rel}} = \frac{2C}{\alpha}$, where C is the constant from Lemma 1, and that $C_{\mathtt{eff}}^{-1} = \sqrt{4 + 2\,||\mathcal{C}^{-1}||}$. We remark that the local indicator θ_T requires the computation of four residuals per element and does not involve the computation of normal nor tangential jumps. Therefore, θ is less expensive and much easier to implement than the a posteriori error estimator proposed in [3]. Moreover, θ can be used in two- and three-dimensional problems, and with any finite element subspace of $\mathbf{H}$. Numerical results, including a numerical comparison of θ and the a posteriori error estimator from [3], are given in Section 4.

3. Non-homogeneous Dirichlet boundary conditions

In this section, we obtain two a posteriori error estimators for the augmented mixed finite element method introduced in [12] for the problem of linear elasticity with non-homogeneous Dirichlet boundary conditions. One of them can also be used in the three-dimensional case.

Given a volume force $\mathbf{f} \in [L^2(\Omega)]^d$ and a prescribed displacement $\mathbf{g} \in [H^{1/2}(\Gamma)]^d$, we now consider the problem of determining the displacement $\mathbf{u}$ and the stress tensor $\boldsymbol{\sigma}$ such that:

$$\left\{ \begin{array}{rcll} \boldsymbol{\sigma} & = & \mathcal{C}\,\boldsymbol{\varepsilon}(\mathbf{u}) & \text{in} \quad \Omega, \\ -\mathbf{div}(\boldsymbol{\sigma}) & = & \mathbf{f} & \text{in} \quad \Omega, \\ \mathbf{u} & = & \mathbf{g} & \text{on } \Gamma, \end{array} \right. \tag{18}$$

where $\mathcal{C}$ and $\boldsymbol{\varepsilon}(\mathbf{u})$ are defined in subsection 2.1. In the next subsection, we recall the augmented variational and discrete formulations proposed in [12, 13] to solve problem (18).

3.1. The augmented mixed finite element method

Let κ_1, κ_2, κ_3 and κ_4 be positive parameters. In [12, 13], besides the residuals arising from the constitutive and equilibrium equations and from the relation that defines the rotation in terms of the displacement, the usual dual-mixed variational formulation of problem (18) is enriched with a consistency term that involves the Dirichlet boundary condition. The resulting augmented variational formulation reads: find $(\boldsymbol{\sigma}, \mathbf{u}, \boldsymbol{\gamma}) \in \tilde{\mathbf{H}} := H_0 \times [H^1(\Omega)]^d \times [L^2(\Omega)]^{d\times d}_{\mathtt{skew}}$ such that

$$\tilde{A}((\boldsymbol{\sigma}, \mathbf{u}, \boldsymbol{\gamma}), (\boldsymbol{\tau}, \mathbf{v}, \boldsymbol{\eta})) \,=\, \tilde{F}(\boldsymbol{\tau}, \mathbf{v}, \boldsymbol{\eta}) \qquad \forall\, (\boldsymbol{\tau}, \mathbf{v}, \boldsymbol{\eta}) \in \tilde{\mathbf{H}}\,, \tag{19}$$

where the bilinear form $\tilde{A} : \tilde{\mathbf{H}} \times \tilde{\mathbf{H}} \to \mathbb{R}$ and the linear functional $\tilde{F} : \tilde{\mathbf{H}} \to \mathbb{R}$ are defined by

$$\tilde{A}((\boldsymbol{\sigma}, \mathbf{u}, \boldsymbol{\gamma}), (\boldsymbol{\tau}, \mathbf{v}, \boldsymbol{\eta})) := A((\boldsymbol{\sigma}, \mathbf{u}, \boldsymbol{\gamma}), (\boldsymbol{\tau}, \mathbf{v}, \boldsymbol{\eta})) + \kappa_4 \int_\Gamma \mathbf{u} \cdot \mathbf{v}$$

$$\tilde{F}(\boldsymbol{\tau}, \mathbf{v}, \boldsymbol{\eta}) := F(\boldsymbol{\tau}, \mathbf{v}, \boldsymbol{\eta}) + \langle \boldsymbol{\tau}\, \mathbf{n}, \mathbf{g} \rangle_\Gamma + \kappa_4 \int_\Gamma \mathbf{g} \cdot \mathbf{v} + \kappa_1\, c_{\mathbf{g}} \int_\Gamma \mathbf{v} \cdot \mathbf{n}\,,$$

for any $(\boldsymbol{\sigma}, \mathbf{u}, \boldsymbol{\gamma}), (\boldsymbol{\tau}, \mathbf{v}, \boldsymbol{\eta}) \in \tilde{\mathbf{H}}$, where $A(\cdot, \cdot)$ and $F(\cdot)$ are defined in (3) and (4), respectively, $\mathbf{n}$ is the unit outward normal to Γ and for $\mathbf{w} : \Gamma \to \mathbb{R}^d$, we denote $c_{\mathbf{w}} := \frac{1}{d\,|\Omega|} \int_\Gamma \mathbf{w} \cdot \mathbf{n}$. In what follows, we denote by $||\cdot||_{\tilde{\mathbf{H}}}$ the product norm of $\tilde{\mathbf{H}}$:

$$\|(\boldsymbol{\tau}, \mathbf{v}, \boldsymbol{\eta})\|^2_{\tilde{\mathbf{H}}} := \|\boldsymbol{\tau}\|^2_{H(\mathbf{div}, \Omega)} + \|\mathbf{v}\|^2_{[H^1(\Omega)]^d} + \|\boldsymbol{\eta}\|^2_{[L^2(\Omega)]^{d \times d}}\,, \quad \forall\, (\boldsymbol{\tau}, \mathbf{v}, \boldsymbol{\eta}) \in \tilde{\mathbf{H}}\,.$$

The following properties and results concerning $\tilde{A}(\cdot, \cdot)$ and the augmented variational formulation (19) were proved in [12, 13]. Let κ_0 be the constant of inequality (3.9) in [12] if $d = 2$ or that of inequality (3.5) in [13] if $d = 3$. Assume that the stabilization parameters, κ_1, κ_2, κ_3 and κ_4, are independent of λ and such that $\kappa_1 \in (0, 2\,\mu)$, $\kappa_2 > 0$, $0 < \kappa_3 < \left(\dfrac{\kappa_0}{1 - \kappa_0}\right) \kappa_1$ if $\kappa_0 < 1$ or $\kappa_3 > 0$ if $\kappa_0 \geq 1$, and $\kappa_4 \geq \kappa_1 + \kappa_3$. Then, according to Theorem 3.3 in [12] and Theorem 3.1 in [13], there exist positive constants, $\tilde{M}$ and $\tilde{\alpha}$, independent of λ, such that

$$|\, \tilde{A}((\boldsymbol{\sigma}, \mathbf{u}, \boldsymbol{\gamma}), (\boldsymbol{\tau}, \mathbf{v}, \boldsymbol{\eta}))\, | \;\leq\; \tilde{M}\, \|(\boldsymbol{\sigma}, \mathbf{u}, \boldsymbol{\gamma})\|_{\tilde{\mathbf{H}}}\, \|(\boldsymbol{\tau}, \mathbf{v}, \boldsymbol{\eta})\|_{\tilde{\mathbf{H}}}\,,$$

for all $(\boldsymbol{\sigma}, \mathbf{u}, \boldsymbol{\gamma})$, $(\boldsymbol{\tau}, \mathbf{v}, \boldsymbol{\eta}) \in \tilde{\mathbf{H}}$ and

$$\tilde{A}((\boldsymbol{\tau}, \mathbf{v}, \boldsymbol{\eta}), (\boldsymbol{\tau}, \mathbf{v}, \boldsymbol{\eta})) \;\geq\; \tilde{\alpha}\, \|(\boldsymbol{\tau}, \mathbf{v}, \boldsymbol{\eta})\|^2_{\tilde{\mathbf{H}}}, \quad \forall\, (\boldsymbol{\tau}, \mathbf{v}, \boldsymbol{\eta}) \in \tilde{\mathbf{H}}\,.$$

Hence, the augmented formulation (19) is well-posed and there exists a positive constant C, independent of λ, such that

$$\|(\boldsymbol{\sigma}, \mathbf{u}, \boldsymbol{\gamma})\|_{\tilde{\mathbf{H}}} \leq C \left(\|\mathbf{f}\|_{[L^2(\Omega)]^d} + \|\mathbf{g}\|_{[H^{1/2}(\Gamma)]^d} \right).$$

It is important to remark that $\boldsymbol{\sigma} \in H_0$. Therefore, the solution $(\boldsymbol{\sigma}, \mathbf{u}, \boldsymbol{\gamma})$ to the augmented formulation (19) satisfies the modified constitutive equation

$$\boldsymbol{\varepsilon}(\mathbf{u}) - \mathcal{C}^{-1} \boldsymbol{\sigma} = c_{\mathbf{g}} \mathbf{I} \qquad \text{in} \quad \Omega, \tag{20}$$

or equivalently, using the definition of the rotation $\boldsymbol{\gamma}$,

$$\nabla \mathbf{u} - \boldsymbol{\gamma} - \mathcal{C}^{-1}\boldsymbol{\sigma} \,=\, c_{\mathbf{g}}\mathbf{I} \qquad \text{in} \quad \Omega. \tag{21}$$

Identities (20) and (21) allow to understand the residual character of some terms involved in the definition of the a posteriori error estimates derived in the next subsection.

Now, let h be a positive parameter and consider a finite dimensional subspace $\tilde{\mathbf{H}}_h \subset \tilde{\mathbf{H}}$. Then, the Galerkin scheme associated to problem (19) reads: find $(\boldsymbol{\sigma}_h, \mathbf{u}_h, \boldsymbol{\gamma}_h) \in \tilde{\mathbf{H}}_h$ such that

$$\tilde{A}((\boldsymbol{\sigma}_h, \mathbf{u}_h, \boldsymbol{\gamma}_h), (\boldsymbol{\tau}_h, \mathbf{v}_h, \boldsymbol{\eta}_h)) \,=\, \tilde{F}(\boldsymbol{\tau}_h, \mathbf{v}_h, \boldsymbol{\eta}_h)\,, \quad \forall\, (\boldsymbol{\tau}_h, \mathbf{v}_h, \boldsymbol{\eta}_h) \in \tilde{\mathbf{H}}_h\,. \tag{22}$$

Problem (22) is well-posed and a Céa estimate can be established (see Theorem 4.1 in [12] and Section 4 in [13]). In this case, the simplest choice of finite element subspaces for the Galerkin scheme (22) is $\tilde{\mathbf{H}}_h \,:=\, H_h^{\boldsymbol{\sigma}} \times H_h^{\mathbf{u}} \times H_h^{\boldsymbol{\gamma}}$, where $H_h^{\boldsymbol{\sigma}}$ and $H_h^{\boldsymbol{\gamma}}$ are the finite element subspaces defined in (7) and (8), respectively, and the finite element subspace $H_h^{\mathbf{u}}$ is defined as follows:

$$H_h^{\mathbf{u}} := \left\{ \mathbf{v}_h \,\in [\mathcal{C}(\bar{\Omega})]^d \,:\, \mathbf{v}_h|_T \,\in [\mathcal{P}_1(T)]^d\,, \quad \forall\, T \,\in\, \mathcal{T}_h \right\}, \tag{23}$$

where $\{\mathcal{T}_h\}_{h>0}$ is a regular family of meshes of Ω, as described in subsection 2.1. For this particular choice, if the solution to problem (19) is sufficiently smooth, a rate of convergence result analogous to (9) can be obtained (see Theorem 4.2 in [12] and Theorem 4.1 in [13]).

3.2. A posteriori error analysis

In this section we derive two new a posteriori error estimators for the Galerkin scheme (22). In what follows, given an element $T \in \mathcal{T}_h$, we denote by $E(T)$ the set of its edges if $d = 2$ (faces if $d = 3$); E_h denotes the set of all the edges/faces of the mesh $\mathcal{T}_h$ and $E_h(\Gamma) := \{e \in E_h \,:\, e \subseteq \Gamma\}$. Finally, h_e stands for the length of edge $e \in E_h$ if $d = 2$. We also assume that problems (19) and (22) are well-posed.

Let $(\boldsymbol{\sigma}, \mathbf{u}, \boldsymbol{\gamma})$ and $(\boldsymbol{\sigma}_h, \mathbf{u}_h, \boldsymbol{\gamma}_h) \in \tilde{\mathbf{H}}_h$ be the unique solutions to problems (19) and (22), respectively. Then, we proceed as in subsection 2.2 and define the Ritz projection of the error as the unique $(\bar{\boldsymbol{\sigma}}, \bar{\mathbf{u}}, \bar{\boldsymbol{\gamma}}) \in \tilde{\mathbf{H}}$ such that

$$\langle (\bar{\boldsymbol{\sigma}}, \bar{\mathbf{u}}, \bar{\boldsymbol{\gamma}}), (\boldsymbol{\tau}, \mathbf{v}, \boldsymbol{\eta}) \rangle_{\tilde{\mathbf{H}}} \,=\, \widetilde{A}((\boldsymbol{\sigma} - \boldsymbol{\sigma}_h, \mathbf{u} - \mathbf{u}_h, \boldsymbol{\gamma} - \boldsymbol{\gamma}_h), (\boldsymbol{\tau}, \mathbf{v}, \boldsymbol{\eta}))\,,$$

for all $(\boldsymbol{\tau},\mathbf{v},\boldsymbol{\eta})\in\tilde{\mathbf{H}}$, where for any $(\boldsymbol{\zeta},\mathbf{w},\boldsymbol{\rho})$, $(\boldsymbol{\tau},\mathbf{v},\boldsymbol{\eta})\in\tilde{\mathbf{H}}$,

$$\langle(\boldsymbol{\zeta},\mathbf{w},\boldsymbol{\rho}),(\boldsymbol{\tau},\mathbf{v},\boldsymbol{\eta})\rangle_{\tilde{\mathbf{H}}} := (\boldsymbol{\zeta},\boldsymbol{\tau})_{H(\mathbf{div};\Omega)} + (\mathbf{w},\mathbf{v})_{[H^1(\Omega)]^d} + (\boldsymbol{\rho},\boldsymbol{\eta})_{[L^2(\Omega)]^{d\times d}}\,.$$

The existence and uniqueness of $(\bar{\boldsymbol{\sigma}},\bar{\mathbf{u}},\bar{\boldsymbol{\gamma}})$ is a consequence of the Lax-Milgram Lemma.

Now, using the coercivity of $\widetilde{A}(\cdot,\cdot)$, we deduce that

$$||(\boldsymbol{\sigma}-\boldsymbol{\sigma}_h,\mathbf{u}-\mathbf{u}_h,\boldsymbol{\gamma}-\boldsymbol{\gamma}_h)||_{\tilde{\mathbf{H}}} \leq \frac{1}{\tilde{\alpha}}\,||(\bar{\boldsymbol{\sigma}},\bar{\mathbf{u}},\bar{\boldsymbol{\gamma}})||_{\tilde{\mathbf{H}}}\,. \tag{24}$$

Lemma 5. *There exists a constant $C>0$, independent of h and λ, such that*

$$\begin{aligned}||(\bar{\boldsymbol{\sigma}},\bar{\mathbf{u}},\bar{\boldsymbol{\gamma}})||_{\tilde{\mathbf{H}}} \leq C\,\Big(&||\mathbf{f}+\mathbf{div}(\boldsymbol{\sigma}_h)||_{[L^2(\Omega)]^d} + ||\boldsymbol{\sigma}_h-\boldsymbol{\sigma}_h^{\mathtt{t}}||_{[L^2(\Omega)]^{d\times d}}\\ &+||\mathbf{g}-\mathbf{u}_h||_{[H^{1/2}(\Gamma)]^d} + ||\boldsymbol{\varepsilon}(\mathbf{u}_h)-\mathcal{C}^{-1}\boldsymbol{\sigma}_h-c_{\mathbf{g}}\mathbf{I}||_{[L^2(\Omega)]^{d\times d}}\\ &+\Big|\Big|\boldsymbol{\gamma}_h-\frac{1}{2}(\nabla\mathbf{u}_h-(\nabla\mathbf{u}_h)^{\mathtt{t}})\Big|\Big|_{[L^2(\Omega)]^{d\times d}}\Big).\end{aligned}$$

Proof. Proceeding similarly as in the proof of Lemma 1, we have that

$$\left\{\begin{array}{rcll}(\bar{\boldsymbol{\sigma}},\boldsymbol{\tau})_{H(\mathbf{div};\Omega)} &=& \widetilde{F}_1(\boldsymbol{\tau}), & \forall\,\boldsymbol{\tau}\in H_0\,,\\ (\bar{\mathbf{u}},\mathbf{v})_{[H^1(\Omega)]^d} &=& \widetilde{F}_2(\mathbf{v}), & \forall\,\mathbf{v}\in[H^1(\Omega)]^d\,,\\ (\bar{\boldsymbol{\gamma}},\boldsymbol{\eta})_{[L^2(\Omega)]^{d\times d}} &=& \widetilde{F}_3(\boldsymbol{\eta}), & \forall\,\boldsymbol{\eta}\in[L^2(\Omega)]^{d\times d}_{\mathtt{skew}}\,,\end{array}\right.$$

where the bounded linear functionals $\widetilde{F}_1$, $\widetilde{F}_2$ and $\widetilde{F}_3$ are defined by

$$\begin{aligned}\widetilde{F}_1(\boldsymbol{\tau}) :=\ & -\kappa_2\int_\Omega(\mathbf{f}+\mathbf{div}(\boldsymbol{\sigma}_h))\cdot\mathbf{div}(\boldsymbol{\tau}) - \int_\Omega(\mathcal{C}^{-1}\boldsymbol{\sigma}_h+\boldsymbol{\gamma}_h):\boldsymbol{\tau}\\ &-\int_\Omega\mathbf{u}_h\cdot\mathbf{div}(\boldsymbol{\tau}) - \kappa_1\int_\Omega(\boldsymbol{\varepsilon}(\mathbf{u}_h)-\mathcal{C}^{-1}\boldsymbol{\sigma}_h):\mathcal{C}^{-1}\boldsymbol{\tau} + \langle\boldsymbol{\tau}\mathbf{n},\mathbf{g}\rangle_\Gamma\,,\end{aligned}$$

$$\begin{aligned}\widetilde{F}_2(\mathbf{v}) :=& \int_\Omega(\mathbf{f}+\mathbf{div}(\boldsymbol{\sigma}_h))\cdot\mathbf{v} - \kappa_1\int_\Omega\big(\boldsymbol{\varepsilon}(\mathbf{u}_h)-\mathcal{C}^{-1}\boldsymbol{\sigma}_h\big):\boldsymbol{\varepsilon}(\mathbf{v})\\ &-\kappa_3\int_\Omega(\boldsymbol{\gamma}_h-\frac{\nabla\mathbf{u}_h-(\nabla\mathbf{u}_h)^{\mathtt{t}}}{2}):\frac{\nabla\mathbf{v}-(\nabla\mathbf{v})^{\mathtt{t}}}{2} + \kappa_4\int_\Gamma(\mathbf{g}-\mathbf{u}_h)\cdot\mathbf{v}\\ &+\kappa_1\,c_{\mathbf{g}}\int_\Gamma\mathbf{v}\cdot\mathbf{n}\,,\end{aligned}$$

$$\widetilde{F}_3(\boldsymbol{\eta}) := \int_\Omega \frac{\boldsymbol{\sigma}_h - \boldsymbol{\sigma}_h^{\mathtt{t}}}{2} : \boldsymbol{\eta} - \kappa_3 \int_\Omega (\boldsymbol{\gamma}_h - \frac{\nabla \mathbf{u}_h - (\nabla \mathbf{u}_h)^{\mathtt{t}}}{2}) : \boldsymbol{\eta}\,.$$

Integrating by parts in the third term in $\widetilde{F}_1$ and using that $\int_\Omega c_{\mathbf{g}}\mathbf{I} : \boldsymbol{\tau} = 0$ when $\boldsymbol{\tau} \in H_0$, we can write

$$\begin{aligned}\widetilde{F}_1(\boldsymbol{\tau}) = &-\kappa_2 \int_\Omega (\mathbf{f} + \mathbf{div}(\boldsymbol{\sigma}_h)) \cdot \mathbf{div}(\boldsymbol{\tau}) - \int_\Omega (\mathcal{C}^{-1}\boldsymbol{\sigma}_h - \nabla \mathbf{u}_h + \boldsymbol{\gamma}_h + c_{\mathbf{g}}\mathbf{I}) : \boldsymbol{\tau} \\ &-\kappa_1 \int_\Omega \mathcal{C}^{-1}(\boldsymbol{\varepsilon}(\mathbf{u}_h) - \mathcal{C}^{-1}\boldsymbol{\sigma}_h - c_{\mathbf{g}}\mathbf{I}) : \boldsymbol{\tau} + \langle \boldsymbol{\tau}\mathbf{n}, \mathbf{g} - \mathbf{u}_h\rangle_\Gamma.\end{aligned}$$

On the other hand, using that $\displaystyle\int_\Gamma \mathbf{v}\cdot\mathbf{n} = \int_\Omega \mathbf{I} : \nabla \mathbf{v} = \int_\Omega \mathbf{I} : \boldsymbol{\varepsilon}(\mathbf{v})$ and (13), we have

$$\begin{aligned}\widetilde{F}_2(\mathbf{v}) &= \int_\Omega (\mathbf{f} + \mathbf{div}(\boldsymbol{\sigma}_h)) \cdot \mathbf{v} - \kappa_1 \int_\Omega (\boldsymbol{\varepsilon}(\mathbf{u}_h) - \mathcal{C}^{-1}\boldsymbol{\sigma}_h - c_{\mathbf{g}}\mathbf{I}) : \boldsymbol{\varepsilon}(\mathbf{v}) \\ &- \kappa_3 \int_\Omega (\boldsymbol{\gamma}_h - \frac{\nabla \mathbf{u}_h - (\nabla \mathbf{u}_h)^{\mathtt{t}}}{2}) : \nabla \mathbf{v} + \kappa_4 \int_\Gamma (\mathbf{g} - \mathbf{u}_h)\cdot \mathbf{v}\,.\end{aligned}$$

Then, the result follows using the Cauchy-Schwarz inequality and the continuity of $\mathcal{C}^{-1}$. □

It is important to remark that, since $\mathbf{u}_h$ is not necessarily zero on Γ, the bound given in Lemma 5 does not reduce to the one given in Lemma 1 when $\mathbf{g} \equiv \mathbf{0}$. Now, motivated by (24) and the previous Lemma, we define

$$\tilde{\theta} := \Big(\sum_{T\in\mathcal{T}_h} \tilde{\theta}_T^2 + ||\mathbf{g} - \mathbf{u}_h||^2_{[H^{1/2}(\Gamma)]^d} \Big)^{1/2},$$

where

$$\begin{aligned}\tilde{\theta}_T^2 := &\ ||\mathbf{f} + \mathbf{div}(\boldsymbol{\sigma}_h)||^2_{[L^2(T)]^d} + ||\boldsymbol{\sigma}_h - \boldsymbol{\sigma}_h^{\mathtt{t}}||^2_{[L^2(T)]^{d\times d}} \\ &+ ||\boldsymbol{\varepsilon}(\mathbf{u}_h) - \mathcal{C}^{-1}\boldsymbol{\sigma}_h - c_{\mathbf{g}}\mathbf{I}||^2_{[L^2(T)]^{d\times d}} + \big|\big|\boldsymbol{\gamma}_h - \tfrac{1}{2}(\nabla \mathbf{u}_h - (\nabla \mathbf{u}_h)^{\mathtt{t}})\big|\big|^2_{[L^2(T)]^{d\times d}}.\end{aligned} \tag{25}$$

It is not difficult to see that $\tilde{\theta}$ is equivalent to the total error. However, the non-local character of the $[H^{1/2}(\Gamma)]^d$-norm makes $\tilde{\theta}$ unuseful in an adaptive refinement algorithm. In the next Theorem, we use an interpolation argument to obtain a reliable and fully local a posteriori error estimator.

Theorem 6. *Assume that* $\mathbf{g} \in [H^1(\Gamma)]^d$. *Then, there exists a constant* $C_{\mathtt{rel}} > 0$, *independent of* h *and* λ, *such that*

$$||(\boldsymbol{\sigma} - \boldsymbol{\sigma}_h, \mathbf{u} - \mathbf{u}_h, \boldsymbol{\gamma} - \boldsymbol{\gamma}_h)||_{\tilde{\mathbf{H}}} \leq C_{\mathtt{rel}}\, \hat{\theta}\,,$$

where $\hat{\theta} := \Big(\sum_{T \in \mathcal{T}_h} \hat{\theta}_T^2 \Big)^{1/2}$, *with* $\hat{\theta}_T^2 := \tilde{\theta}_T^2 + \sum_{e \in E(T) \cap E_h(\Gamma)} ||\mathbf{g} - \mathbf{u}_h||^2_{[H^1(e)]^d}$.

Proof. Using that $[H^{1/2}(\Gamma)]^d$ is the interpolation space of index $1/2$ between $[L^2(\Gamma)]^d$ and $[H^1(\Gamma)]^d$, we have that

$$\begin{aligned} ||\mathbf{g} - \mathbf{u}_h||^2_{[H^{1/2}(\Gamma)]^d} &\leq C\, ||\mathbf{g} - \mathbf{u}_h||_{[L^2(\Gamma)]^d} ||\mathbf{g} - \mathbf{u}_h||_{[H^1(\Gamma)]^d} \\ &\leq C \sum_{e \in E_h(\Gamma)} ||\mathbf{g} - \mathbf{u}_h||^2_{[H^1(e)]^d}\,. \end{aligned}$$

The result follows from (24), Lemma 5, (25) and the previous inequality. □

In what follows, we assume that $d = 2$ and that $H_h^{\mathbf{u}}$ is given by (23). Then, we follow [2] and let $\bar{\mathbf{u}}_h$ be the unique continuous piecewise-linear function in $\mathcal{T}_h$ such that $\bar{\mathbf{u}}_h(\mathbf{x}) = \mathbf{u}_h(\mathbf{x})$ for any node $\mathbf{x}$ of $\mathcal{T}_h$ in Ω and $\bar{\mathbf{u}}_h(\mathbf{x}) = \mathbf{g}(\mathbf{x})$ for any node $\mathbf{x}$ of $\mathcal{T}_h$ on Γ. Let $\kappa := \max\Big\{ \frac{h_{e_i}}{h_{e_j}} : e_i \text{ neighbor of } e_j,\ i,j = 1,\ldots,n \Big\}$, where $\{e_i\}_{i=1}^n$ is the partition of Γ induced by $\mathcal{T}_h$. Then, by virtue of Theorem 1 in [6], if $\mathbf{g} \in [H^1(\Gamma)]^2$, there exists a constant $C > 0$, independent of h and λ, such that

$$||\mathbf{g} - \bar{\mathbf{u}}_h||^2_{[H^{1/2}(\Gamma)]^2} \leq C\, \log(1+\kappa) \sum_{e \in E_h(\Gamma)} h_e \left|\left| \frac{\mathrm{d}\mathbf{g}}{\mathrm{d}\mathbf{t}_T} - \frac{\mathrm{d}\bar{\mathbf{u}}_h}{\mathrm{d}\mathbf{t}_T} \right|\right|^2_{[L^2(e)]^2}, \qquad (26)$$

where $\frac{\mathrm{d}}{\mathrm{d}\mathbf{t}_T}$ denotes the tangential derivative.

Remark 7. *The tangential derivative* $\frac{\mathrm{d}}{\mathrm{d}\mathbf{t}} : H^1(D) \to H^{-1/2}(\partial D)$ *is a linear continuous operator, where* $D \subset \mathbb{R}^2$ *is a Lipschitz-continuous domain. Indeed, we know from [14, page 253] that the tangential trace is continuous as a mapping from* $H(\mathrm{curl}; D)$ *into* $H^{-1/2}(\partial D)$. *Then, the result follows by using that if* $u \in H^1(D)$, *then* $\nabla u \in H(\mathrm{curl}; D)$ *and* $||\nabla u||_{H(\mathrm{curl};D)} = |u|_{1,D}$ *(because* $\mathrm{curl}\, \nabla u = 0$ *in* D*).*

We also have the following Lemma.

Lemma 8. *Assume that each component of* $\mathbf{g}$ *is a piecewise polynomial on* $\{e_i\}_{i=1}^n$. *Then, there exists a constant* $C > 0$, *independent of* h *and* λ, *such that*

$$h_e \left|\left| \frac{\mathrm{d}\mathbf{g}}{\mathrm{d}\mathbf{t}_T} - \frac{\mathrm{d}\bar{\mathbf{u}}_h}{\mathrm{d}\mathbf{t}_T} \right|\right|^2_{[L^2(e)]^2} \leq C \, ||\mathbf{u} - \bar{\mathbf{u}}_h||^2_{[H^1(T_e)]^2}, \qquad \forall \, e \in E_h(\Gamma) \, ,$$

where T_e *is the triangle in* $\mathcal{T}_h$ *that has* e *as an edge.*

Proof. The result follows by applying the inverse inequality (2.1.30) in [1] with $\tau = -1/2$ and $\sigma = 0$, using the definition of the norm $||\cdot||_{H^{-1/2}(e)}$ (see, for instance, [6]), and the continuity of the tangential derivative operator from $[H^1(T_e)]^2$ to $[H^{-1/2}(\partial T_e)]^2$ (see Remark 7). □

Then, we may define the a posteriori error estimate $\bar{\theta} := \Big(\sum_{T \in \mathcal{T}_h} \bar{\theta}_T^2 \Big)^{1/2}$, where

$$\begin{aligned} \bar{\theta}_T^2 := {} & ||\mathbf{f} + \mathbf{div}(\boldsymbol{\sigma}_h)||^2_{[L^2(T)]^2} \, + \, ||\boldsymbol{\sigma}_h - \boldsymbol{\sigma}_h^{\mathtt{t}}||^2_{[L^2(T)]^{2\times 2}} + ||\mathbf{u}_h - \bar{\mathbf{u}}_h||^2_{[H^1(T)]^2} \\ + \left|\left| \boldsymbol{\gamma}_h - \frac{1}{2} \left(\nabla \mathbf{u}_h - (\nabla \mathbf{u}_h)^{\mathtt{t}} \right) \right|\right|^2_{[L^2(T)]^{2\times 2}} & + \, \left|\left| \boldsymbol{\varepsilon}(\mathbf{u}_h) - \mathcal{C}^{-1} \boldsymbol{\sigma}_h - c_{\mathbf{g}} \mathbf{I} \right|\right|^2_{[L^2(T)]^{2\times 2}} \\ & + \log(1+\kappa) \sum_{e \in E(T) \cap E_h(\Gamma)} h_e \left|\left| \frac{\mathrm{d}\mathbf{g}}{\mathrm{d}\mathbf{t}_T} - \frac{\mathrm{d}\bar{\mathbf{u}}_h}{\mathrm{d}\mathbf{t}_T} \right|\right|^2_{[L^2(e)]^2} . \end{aligned} \tag{27}$$

Theorem 9. *If* $\mathbf{g} \in [H^1(\Gamma)]^2$, *then there exists a constant* $C_{\mathtt{rel}} > 0$, *independent of* h *and* λ, *such that*

$$||(\boldsymbol{\sigma} - \boldsymbol{\sigma}_h, \mathbf{u} - \mathbf{u}_h, \boldsymbol{\gamma} - \boldsymbol{\gamma}_h)||_{\tilde{\mathbf{H}}} \leq C_{\mathtt{rel}} \, \bar{\theta} \, .$$

If, moreover, each component of $\mathbf{g}$ *is a piecewise polynomial on* Γ, *then there exists a positive constant* $C_{\mathtt{eff}}$, *independent of* h *and* λ, *such that*

$$C_{\mathtt{eff}} \, \bar{\theta}_T^2 \leq ||(\boldsymbol{\sigma} - \boldsymbol{\sigma}_h, \mathbf{u} - \mathbf{u}_h, \boldsymbol{\gamma} - \boldsymbol{\gamma}_h)||^2_{\mathbf{H}(T)} \, + \, \chi(T) \, ||\mathbf{u}_h - \bar{\mathbf{u}}_h||^2_{[H^1(T)]^2} \, ,$$

for all $T \in \mathcal{T}_h$, *where* $\chi(T)$ *is equal to* 1 *if* $\partial T \cap \Gamma \neq \emptyset$ *and is equal to* 0 *otherwise.*

Proof. The reliability follows from (24), Lemma 5, the triangle inequality, (26), a trace inequality and the definition of $\bar{\theta}$. On the other hand, let $T \in \mathcal{T}_h$.

If $T \subset \Omega$, then $\mathbf{u}_h = \bar{\mathbf{u}}_h$ in T and the third and sixth terms in (27) vanish. In this case, the result follows straightforwardly. If $\partial T \cap \Gamma \neq \emptyset$, the result follows by applying Lemma 8. $\square$

We remark that the a posteriori error estimator $\bar{\theta}$ is locally efficient in the interior elements (that is, those that do not touch the boundary). Besides, the computation of $\bar{\theta}$ involves four residuals per element in the interior triangles, five residuals per element in the triangles with exactly one vertex on the boundary and six residuals per element in the triangles with a side on the boundary. We emphasize that $\bar{\theta}$ has been derived in the two-dimensional setting, assuming that displacements are approximated by continuous piecewise linear finite elements. In the next section, we provide some numerical results illustrating the performance of the corresponding adaptive method, including a numerical comparison with the a posteriori error estimator proposed in [4].

4. Numerical experiments

In this section we present some numerical results that illustrate the performance of the discrete schemes (6) and (22), and that of the adaptive algorithms based on the a posteriori error estimators θ, $\hat{\theta}$ and $\bar{\theta}$ when the simplest finite element subspaces are used to solve the linear elasticity problem in the plane. We implemented the augmented discrete schemes following the ideas in Section 4.3 of [11]. The numerical experiments were carried out in a notebook *Intel Core i7-820QM* with four dual processors using a Matlab code.

We recall that given the Young modulus E and the Poisson ratio ν of a linear elastic material, the corresponding Lamé parameters are defined by $\mu := \frac{E}{2(1+\nu)}$ and $\lambda := \frac{E\,\nu}{(1+\nu)\,(1-2\,\nu)}$. In the examples below, we take $E = 1$ and consider the values $\nu = 0.4900$ and $\nu = 0.4999$, which yield the following values of μ and λ:

ν	μ	λ
0.4900	0.3356	16.4430
0.4999	0.3334	1666.4444

Given an error indicator $\zeta := (\sum_{T \in \mathcal{T}_h} \zeta_T^2)^{1/2}$, we consider the following adaptive algorithm:

1. Start with a coarse mesh $\mathcal{T}_h$.
2. Solve the Galerkin scheme for the current mesh $\mathcal{T}_h$.

3. Compute ζ_T for each triangle $T \in \mathcal{T}_h$.
4. Consider stopping criterion and decide to finish or go to the next step.
5. Use *blue-green* refinement to refine each element $T' \in \mathcal{T}_h$ such that

$$\zeta_{T'} \geq \frac{1}{2} \max\{ \zeta_T : T \in \mathcal{T}_h \}.$$

6. Define the resulting mesh as the new $\mathcal{T}_h$ and go to step 2.

In what follows, $\mathcal{N}$ denotes the total number of dof for the corresponding discrete scheme. We define the error in each unknown, $e(\boldsymbol{\sigma}) := \|\boldsymbol{\sigma} - \boldsymbol{\sigma}_h\|_{H(\mathbf{div};\Omega)}$, $e(\mathbf{u}) := \|\mathbf{u} - \mathbf{u}_h\|_{[H^1(\Omega)]^2}$ and $e(\boldsymbol{\gamma}) := \|\boldsymbol{\gamma} - \boldsymbol{\gamma}_h\|_{[L^2(\Omega)]^{2\times 2}}$. The individual errors are computed using a Gaussian quadrature rule on each triangle. Then, the total error is given by $e(\boldsymbol{\sigma}, \mathbf{u}, \boldsymbol{\gamma}) := \left(e(\boldsymbol{\sigma})^2 + e(\mathbf{u})^2 + e(\boldsymbol{\gamma})^2 \right)^{1/2}$. The efficiency index of an error indicator ζ is defined as $I(\zeta) := e(\boldsymbol{\sigma}, \mathbf{u}, \boldsymbol{\gamma})/\zeta$. Finally, we define the experimental rate of convergence as

$$r(e(\boldsymbol{\sigma}, \mathbf{u}, \boldsymbol{\gamma})) := -2 \frac{\log(e(\boldsymbol{\sigma}, \mathbf{u}, \boldsymbol{\gamma})/e(\boldsymbol{\sigma}, \mathbf{u}, \boldsymbol{\gamma})')}{\log(\mathcal{N}/\mathcal{N}')},$$

where $\mathcal{N}$ and $\mathcal{N}'$ denote the dof of two consecutive triangulations, and $e(\boldsymbol{\sigma}, \mathbf{u}, \boldsymbol{\gamma})$ and $e(\boldsymbol{\sigma}, \mathbf{u}, \boldsymbol{\gamma})'$ are the corresponding total errors.

4.1. Homogeneous boundary conditions

In this section we show some numerical results that illustrate the performance of the discrete scheme (6) and of the adaptive algorithm based on the a posteriori error estimator θ. In the table below we specify the examples to be considered here. The domain Ω will be either the unit square $]0,1[^2$ or the L-shaped domain $]-0.5, 0.5[^2 \setminus [0, 0.5]^2$, and we choose $\mathbf{f}$ so that the exact solution is $\mathbf{u}(x_1, x_2) := (u_1(x_1, x_2), u_2(x_1, x_2))^{\mathtt{t}}$ as specified below. Since the augmented method is robust with respect to the stabilization parameters (see [11]), we take $\bar{\kappa} = \left(\mu, \frac{1}{2\mu}, \frac{\mu}{2}\right)$ in all the examples, which is a feasible choice.

Ex.	Ω	ν	$u_1(x_1, x_2) \;=\; u_2(x_1, x_2)$
1	Square	0.4900 0.4999	$\dfrac{x_1\,(x_1-1)\,x_2\,(x_2-1)}{(x_1-1)^2+(x_2-1)^2+0.01}$
2	L-shape	0.4900	$x_1\,x_2\,(x_1^2-0.25)\,(x_2^2-0.25)\,(x_1^2+x_2^2)^{-1/3}$
3	L-shape	0.4900	$x_1\,x_2\,(x_1^2-0.25)\,(x_2^2-0.25)\,(x_1^2+10^{-4})^{-1/3}$

We first emphasize the robustness of the a posteriori error estimator θ with respect to the Poisson ratio. We approximate the solution of Example 1 for two different values of ν using a sequence of uniform meshes. Hereafter, uniform refinement means that given a uniform initial triangulation, each subsequent mesh is obtained from the previous one by dividing each triangle into the four ones arising when connecting the midpoints of its sides. In Tables I and II we present the individual and total errors, the experimental convergence rates, the a posteriori error estimators and the efficiency indices obtained for Example 1 with $\nu = 0.4900$ and $\nu = 0.4999$, respectively.

Table I: Dof, individual and total errors, convergence rate, a posteriori error estimator and efficiency index for a sequence of uniform meshes (EXAMPLE 1, $\nu = 0.4900$).

$\mathcal{N}$	$e(\boldsymbol{\sigma})$	$e(\mathbf{u})$	$e(\boldsymbol{\gamma})$	$e(\boldsymbol{\sigma},\mathbf{u},\boldsymbol{\gamma})$	$r(e(\boldsymbol{\sigma},\mathbf{u},\boldsymbol{\gamma}))$	θ	$I(\theta)$
323	0.8866E+2	0.3696E+1	0.1226E+2	0.8958E+2	—-	0.9041E+2	0.9907
1283	0.7139E+2	0.2280E+1	0.7457E+1	0.7181E+2	0.3205	0.7221E+2	0.9946
5123	0.3390E+2	0.1124E+1	0.5477E+1	0.3435E+2	1.0651	0.3478E+2	0.9878
20483	0.1729E+2	0.5606E+0	0.3926E+1	0.1774E+2	0.9539	0.1817E+2	0.9764
81923	0.8684E+1	0.2116E+0	0.2407E+1	0.9014E+1	0.9767	0.9337E+1	0.9654
327683	0.4345E+1	0.6771E-1	0.1306E+1	0.4537E+1	0.9903	0.4728E+1	0.9597

Table II: Dof, individual and total errors, convergence rate, a posteriori error estimator and efficiency index for a sequence of uniform meshes (EXAMPLE 1, $\nu = 0.4999$).

$\mathcal{N}$	$e(\boldsymbol{\sigma})$	$e(\mathbf{u})$	$e(\boldsymbol{\gamma})$	$e(\boldsymbol{\sigma},\mathbf{u},\boldsymbol{\gamma})$	$r(e(\boldsymbol{\sigma},\mathbf{u},\boldsymbol{\gamma}))$	θ	$I(\theta)$
323	0.8780E+4	0.3662E+3	0.1246E+4	0.8875E+4	—-	0.8962E+4	0.9903
1283	0.7013E+4	0.2286E+3	0.7552E+3	0.7058E+4	0.3323	0.7098E+4	0.9943
5123	0.3329E+4	0.1153E+3	0.5515E+3	0.3376E+4	1.0653	0.3419E+4	0.9873
20483	0.1697E+4	0.5720E+2	0.3928E+3	0.1743E+4	0.9543	0.1786E+4	0.9756
81923	0.8521E+3	0.2140E+2	0.2398E+3	0.8855E+3	0.9768	0.9181E+3	0.9645
327683	0.4264E+3	0.6647E+1	0.1298E+3	0.4457E+3	0.9903	0.4649E+3	0.9588

We remark that in both cases, independently of the error values, there are practically no differences between the efficiency indices obtained with the two values of ν, which numerically shows the robustness of θ with respect to ν (and hence with respect to the Lamé parameter λ).

Next we consider Examples 2 and 3 to illustrate the performance of the adaptive algorithm based on θ. We remark that the solution to Example 2 is singular at the boundary point $(0,0)$. In fact, the behavior of $\mathbf{u}$ in a neighborhood of the origin implies that $\mathbf{div}(\boldsymbol{\sigma}) \in [H^{1/3}(\Omega)]^2$, so that the expected convergence rate for the uniform refinement is $1/3$. On the other hand, the solution to Example 3 exhibits large stress regions around the line $x_1 = 0$. In Tables III through VI we provide the corresponding individual and total errors, the experimental convergence rates, the a posteriori error estimators and the efficiency indices for the uniform and adaptive refinements.

In Table III we can observe how the convergence rates for the uniform refinement approach $1/3$ in Example 2. In Table IV we observe that the adaptive algorithm is able to recover, at least approximately, the rate of convergence $O(h)$ for the total error. We also remark that the efficiency indices take values around 0.9, which confirms the reliability and efficiency of the a posteriori error estimator θ.

Table III: Dof, individual and total errors, experimental convergence rates, a posteriori error estimators and efficiency indices for the uniform refinement (EXAMPLE 2).

$\mathcal{N}$	$e(\boldsymbol{\sigma})$	$e(\mathbf{u})$	$e(\boldsymbol{\gamma})$	$e(\boldsymbol{\sigma},\mathbf{u},\boldsymbol{\gamma})$	$r(e(\boldsymbol{\sigma},\mathbf{u},\boldsymbol{\gamma}))$	θ	$I(\theta)$
243	0.1310E+1	0.8236E-1	0.4502E+0	0.1388E+1	—	0.1464E+1	0.9480
963	0.8749E+0	0.4975E-1	0.2638E+0	0.9152E+0	0.6047	0.9533E+0	0.9601
3843	0.6287E+0	0.2488E-1	0.1644E+0	0.6503E+0	0.4938	0.6711E+0	0.9691
15363	0.4754E+0	0.1121E-1	0.1022E+0	0.4864E+0	0.4192	0.4973E+0	0.9781
61443	0.3694E+0	0.4095E-2	0.5943E-1	0.3742E+0	0.3783	0.3791E+0	0.9872
245763	0.2907E+0	0.1336E-2	0.3188E-1	0.2924E+0	0.3557	0.2942E+0	0.9939

Table IV: Dof, individual and total errors, experimental convergence rates, a posteriori error estimators and efficiency indices for the adaptive refinement (EXAMPLE 2).

$\mathcal{N}$	$e(\boldsymbol{\sigma})$	$e(\mathbf{u})$	$e(\boldsymbol{\gamma})$	$e(\boldsymbol{\sigma},\mathbf{u},\boldsymbol{\gamma})$	$r(e(\boldsymbol{\sigma},\mathbf{u},\boldsymbol{\gamma}))$	θ	$I(\theta)$
243	0.1310E+1	0.8236E-1	0.4502E+0	0.1388E+1	—	0.1464E+1	0.9480
853	0.8863E+0	0.4802E-1	0.2542E+0	0.9233E+0	0.6491	0.9598E+0	0.9620
1313	0.7479E+0	0.3747E-1	0.2265E+0	0.7823E+0	0.7684	0.8163E+0	0.9584
2273	0.6122E+0	0.3188E-1	0.1127E+0	0.6233E+0	0.8283	0.6351E+0	0.9814
2833	0.5369E+0	0.2916E-1	0.1014E+0	0.5472E+0	1.1828	0.5580E+0	0.9806
3643	0.4662E+0	0.2826E-1	0.9711E-1	0.4770E+0	1.0907	0.4876E+0	0.9784
4483	0.4206E+0	0.2401E-1	0.8663E-1	0.4301E+0	0.9993	0.4390E+0	0.9795
5393	0.3794E+0	0.2225E-1	0.8543E-1	0.3895E+0	1.0710	0.3991E+0	0.9760
6943	0.3355E+0	0.2021E-1	0.7875E-1	0.3452E+0	0.9563	0.3543E+0	0.9743
7963	0.3140E+0	0.1967E-1	0.7499E-1	0.3234E+0	0.9502	0.3323E+0	0.9733
12113	0.2633E+0	0.1743E-1	0.6385E-1	0.2715E+0	0.8351	0.2786E+0	0.9746
15913	0.2246E+0	0.1544E-1	0.5938E-1	0.2328E+0	1.1271	0.2400E+0	0.9700
18963	0.2042E+0	0.1389E-1	0.5392E-1	0.2117E+0	1.0844	0.2182E+0	0.9701
23633	0.1821E+0	0.1194E-1	0.5128E-1	0.1896E+0	1.0025	0.1963E+0	0.9654
29443	0.1649E+0	0.9675E-2	0.4254E-1	0.1706E+0	0.9585	0.1759E+0	0.9702
36023	0.1511E+0	0.9076E-2	0.3389E-1	0.1551E+0	0.9444	0.1588E+0	0.9769
49053	0.1299E+0	0.8420E-2	0.3123E-1	0.1339E+0	0.9524	0.1374E+0	0.9746
63403	0.1128E+0	0.7547E-2	0.2811E-1	0.1165E+0	1.0868	0.1197E+0	0.9730

In Figure 1 we display the total error versus the dof for the uniform refinement and the adaptive refinements based on θ and η, where η is the a posteriori error estimator proposed in [3]. We can observe there that the adaptive procedures converge faster than the uniform one and, in particular, the adaptive algorithm based on θ shows the best performance for this example.

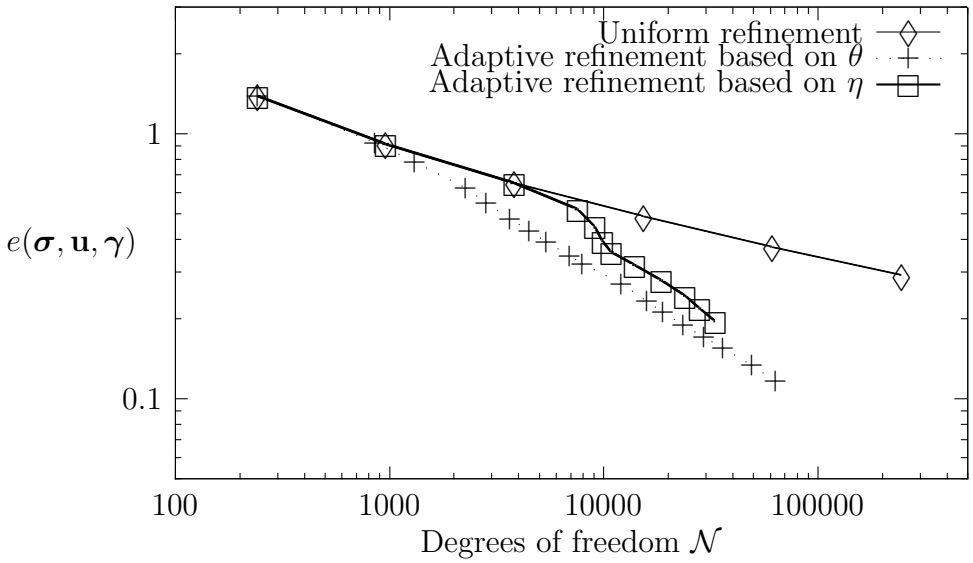

Figure 1: Total error vs. degrees of freedom
for the uniform and adaptive refinements (EXAMPLE 2).

In Figure 2 we display the efficiency indices of the a posteriori error estimators θ and η vs the dof. We remark that the efficiency indices of θ are closer to 1 than those of η. In Figure 3, we display some intermediate meshes obtained with the adaptive algorithm based on θ as applied to Example 2. We remark that the meshes are highly refined in a neighborhood of the singular point.

In Example 3 the solution exhibits large stress regions around the line $x_1 = 0$. In Tables V and VI we provide the corresponding individual and total errors, the experimental convergence rates, the a posteriori error estimators and the efficiency indices for the uniform and adaptive refinements, respectively. We observe that the uniform procedure is unable to attain linear convergence whereas the adaptive procedure based on θ does. This fact can also be noticed in Figure 4, where we display the total error versus the dof for the uniform refinement and the adaptive refinements based on θ and η. In this example, the performance of θ and η is very similar. We also remark from Tables V and VI that the efficiency indices remain bounded in a neighborhood of 0.99, which confirms the reliability and efficiency of the a posteriori error estimator θ.

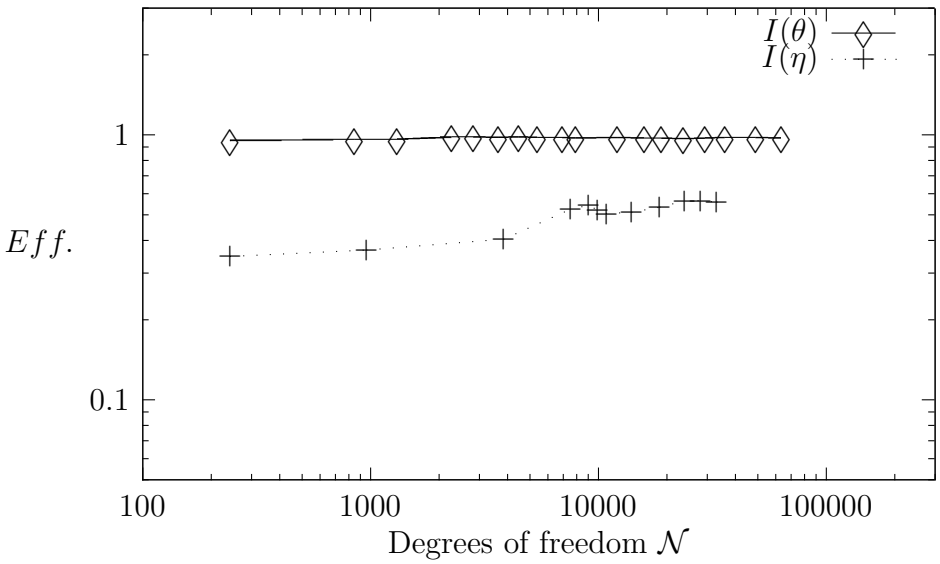

Figure 2: Efficiency indices vs. dof for adaptive refinements (EXAMPLE 2).

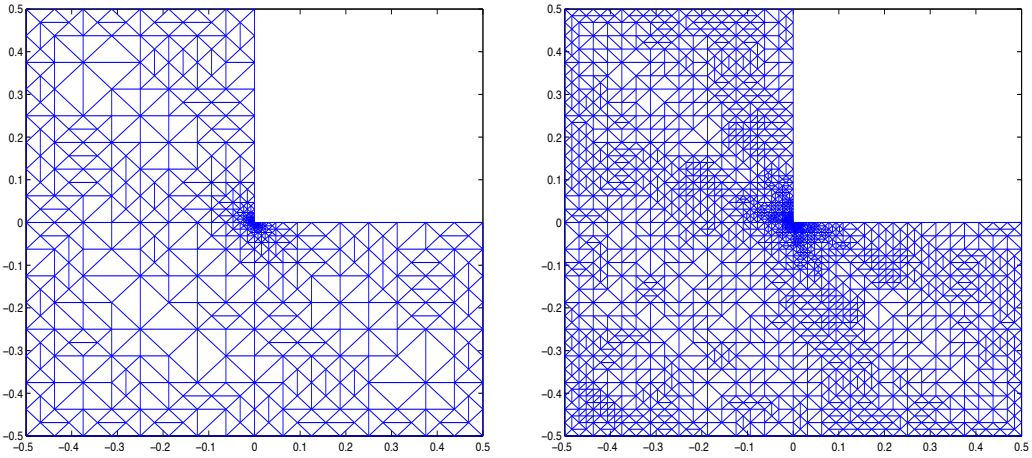

Figure 3: Adapted meshes with 4483 and 18963 dof (EXAMPLE 2).

Table V: Dof, individual and total errors, experimental convergence rates, a posteriori error estimators and efficiency indices for the uniform refinement (EXAMPLE 3).

$\mathcal{N}$	$e(\boldsymbol{\sigma})$	$e(\mathbf{u})$	$e(\boldsymbol{\gamma})$	$e(\boldsymbol{\sigma},\mathbf{u},\boldsymbol{\gamma})$	$r(e(\boldsymbol{\sigma},\mathbf{u},\boldsymbol{\gamma}))$	θ	$I(\theta)$
243	0.2090E+2	0.6142E+0	0.7291E+0	0.2092E+2	—-	0.2096E+2	0.9982
963	0.1880E+2	0.4015E+0	0.4922E+0	0.1881E+2	0.1543	0.1883E+2	0.9991
3843	0.1119E+2	0.1426E+0	0.3528E+0	0.1120E+2	0.7501	0.1121E+2	0.9992
15363	0.7646E+1	0.3972E-1	0.2308E+0	0.7649E+1	0.5499	0.7654E+1	0.9994
61443	0.6237E+1	0.2994E-1	0.1412E+0	0.6238E+1	0.2941	0.6240E+1	0.9997
245763	0.3807E+1	0.1216E-1	0.8152E-1	0.3808E+1	0.7123	0.3809E+1	0.9997

Table VI: Dof, individual and total errors, experimental convergence rates, a posteriori error estimators and efficiency indices for the adaptive refinement (EXAMPLE 3).

$\mathcal{N}$	$e(\boldsymbol{\sigma})$	$e(\mathbf{u})$	$e(\boldsymbol{\gamma})$	$e(\boldsymbol{\sigma},\mathbf{u},\boldsymbol{\gamma})$	$r(e(\boldsymbol{\sigma},\mathbf{u},\boldsymbol{\gamma}))$	θ	$I(\theta)$
243	0.2090E+2	0.6142E+0	0.7291E+0	0.2092E+2	—-	0.2096E+2	0.9982
453	0.1882E+2	0.4123E+0	0.5552E+0	0.1883E+2	0.3384	0.1885E+2	0.9990
873	0.1122E+2	0.1555E+0	0.4570E+0	0.1123E+2	1.5753	0.1125E+2	0.9989
2063	0.7706E+1	0.7550E-1	0.2589E+0	0.7711E+1	0.8749	0.7716E+1	0.9993
4198	0.6420E+1	0.6873E-1	0.2014E+0	0.6423E+1	0.5141	0.6427E+1	0.9994
10558	0.4097E+1	0.4675E-1	0.1616E+0	0.4101E+1	0.9733	0.4104E+1	0.9991
26973	0.2331E+1	0.4153E-1	0.1444E+0	0.2336E+1	1.2000	0.2340E+1	0.9981
74173	0.1359E+1	0.2709E-1	0.1140E+0	0.1364E+1	1.0640	0.1368E+1	0.9966

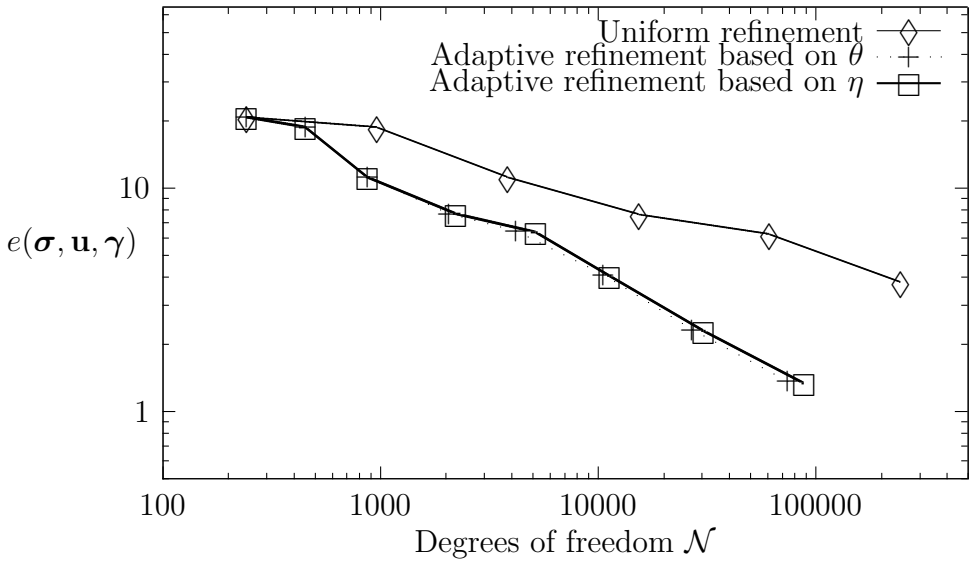

Figure 4: Total error vs. degrees of freedom for the uniform and adaptive refinements (EXAMPLE 3).

In Figure 5 we display the efficiency indices of the a posteriori error estimators θ and η vs the dof as applied to Example 3. Again, the efficiency

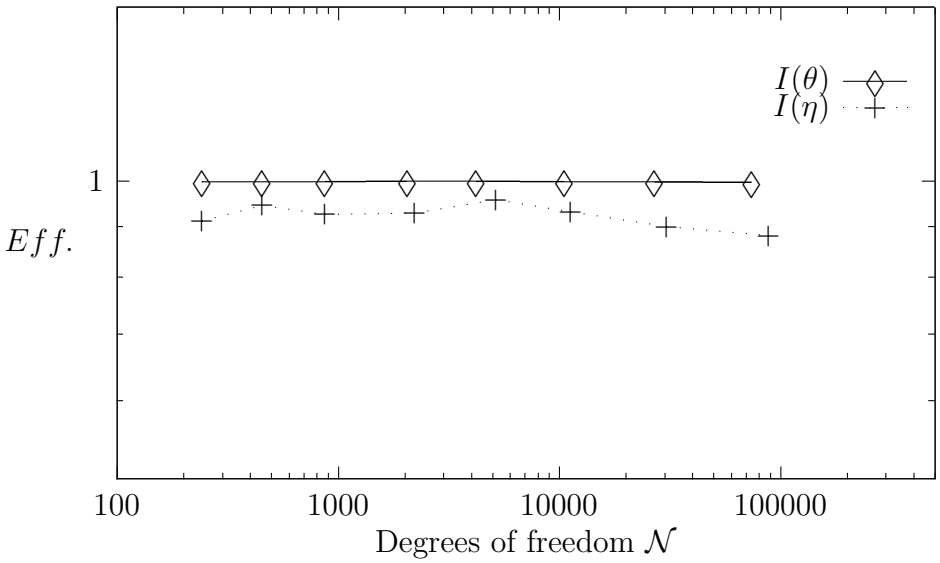

Figure 5: Efficiency indices vs. dof for adaptive refinements (EXAMPLE 3).

indices of θ are closer to 1 than those of η. Finally, we display in Figure 6 some intermediate meshes obtained with the adaptive algorithm based on θ. We remark that the adaptive algorithm is able to recognize the large stress regions of the solution since the adapted meshes are highly refined around the line $x_1 = 0$, where the largest stresses occur.

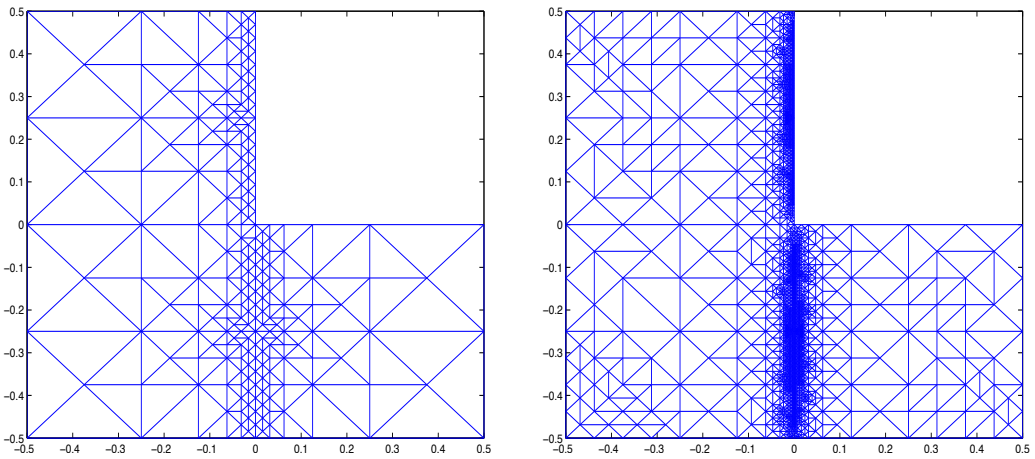

Figure 6: Adapted meshes with 2063 and 26973 dof (EXAMPLE 3).

4.2. Non-homogeneous Dirichlet boundary conditions

In this section we present several numerical results that illustrate the performance of the augmented scheme (22) and the a posteriori error estimators $\hat{\theta}$ and $\bar{\theta}$ for the simplest finite element subspace $\tilde{\mathbf{H}}_h$ defined in Section 3. We consider the following values for the stabilization parameters (cf. [12, 13]):

$$\kappa_1 = \mu, \quad \kappa_2 = \frac{1}{2\,\mu}, \quad \kappa_3 = \frac{1}{8}\kappa_1, \quad \kappa_4 = \kappa_1 + \kappa_3.$$

In the Table below we specify the three examples to be considered in this section. We choose the data $\mathbf{f}$ and $\mathbf{g}$ so that the exact solution is $\mathbf{u}(x_1, x_2) := (u_1(x_1, x_2), u_2(x_1, x_2))^{\mathtt{t}}$.

EXAMPLE	Ω	$u_1(x_1, x_2) = u_2(x_1, x_2)$
4	$]0,1[^2$	$x_1\, x_2\, e^{x_1+x_2}$
5	$]-0.25, 0.25[^2 \backslash [0, 0.25]^2$	$\dfrac{x_1\, x_2}{(x_1^2 + x_2^2)^{1/3}} + 2x_2$
6	$]0,1[^2 \backslash \{\mathbf{x} \in \mathbb{R}^2 \,:\, \|\mathbf{x}\| \leq 0.1\}$	$\dfrac{10^{-4}}{x_1^2 + x_2^2 - 0.05^2}$

We use Example 4 to show the robustness of the a posteriori error estimators $\hat{\theta}$ and $\bar{\theta}$ with respect to the Poisson ratio. In Tables VII and VIII we provide the total error, the experimental convergence rates, the values of the a posteriori error estimators $\hat{\theta}$ and $\bar{\theta}$ and the corresponding efficiency indices for a sequence of uniform meshes, for $\nu = 0.4900$ and $\nu = 0.4999$, respectively. We remark that, independently of how large the errors could become, there are practically no differences between the efficiency indices obtained with the two values of ν, which numerically shows the robustness of the a posteriori error estimators $\hat{\theta}$ and $\bar{\theta}$ with respect to the Poisson ratio (and hence, with respect to the Lamé parameter λ).

Table VII: Dof, total errors, experimental convergence rates, a posteriori error estimators and efficiency indices (uniform refinement) (EXAMPLE 4, $\nu = 0.4900$).

$\mathcal{N}$	$e(\boldsymbol{\sigma}, \mathbf{u}, \boldsymbol{\gamma})$	$r(e(\boldsymbol{\sigma}, \mathbf{u}, \boldsymbol{\gamma}))$	$\hat{\theta}$	$I(\hat{\theta})$	$\bar{\theta}$	$I(\bar{\theta})$
59	0.9332E+2	—	0.1046E+3	0.8925	0.9878E+2	0.9448
195	0.4636E+2	1.1703	0.5291E+2	0.8762	0.5069E+2	0.9146
707	0.2342E+2	1.0602	0.2709E+2	0.8645	0.2624E+2	0.8926
2691	0.1203E+2	0.9975	0.1421E+2	0.8464	0.1390E+2	0.8649
10499	0.6141E+1	0.9873	0.7370E+1	0.8333	0.7265E+1	0.8454
41475	0.3099E+1	0.9955	0.3737E+1	0.8294	0.3700E+1	0.8376
164867	0.1555E+1	0.9998	0.1874E+1	0.8295	0.1861E+1	0.8353
657411	0.7782E+0	1.0007	0.9368E+0	0.8307	0.9323E+0	0.8347

Table VIII: Dof, total errors, experimental convergence rates, a posteriori error estimators and efficiency indices (uniform refinement) (EXAMPLE 4, $\nu = 0.4999$).

$\mathcal{N}$	$e(\boldsymbol{\sigma}, \mathbf{u}, \boldsymbol{\gamma})$	$r(e(\boldsymbol{\sigma}, \mathbf{u}, \boldsymbol{\gamma}))$	$\hat{\theta}$	$I(\hat{\theta})$	$\bar{\theta}$	$I(\bar{\theta})$
59	0.9180E+4	—	0.1015E+5	0.9044	0.9640E+4	0.9522
195	0.4556E+4	1.1718	0.5143E+4	0.8859	0.4949E+4	0.9206
707	0.2297E+4	1.0637	0.2628E+4	0.8739	0.2554E+4	0.8992
2691	0.1176E+4	1.0018	0.1375E+4	0.8554	0.1348E+4	0.8721
10499	0.5996E+3	0.9894	0.7130E+3	0.8410	0.7039E+3	0.8518
41475	0.3025E+3	0.9962	0.3617E+3	0.8362	0.3586E+3	0.8435
164867	0.1517E+3	1.0000	0.1815E+3	0.8359	0.1804E+3	0.8409
657411	0.7593E+2	1.0008	0.9073E+2	0.8369	0.9037E+2	0.8402

Next, we use Example 4 to illustrate the behavior of the boundary terms in $\hat{\theta}$ and $\bar{\theta}$. We define

$$\hat{\theta}_\Gamma := \left(\sum_{T \in \mathcal{T}_h} \sum_{e \in E(T) \cap E_h(\Gamma)} ||\mathbf{g} - \mathbf{u}_h||^2_{[H^1(e)]^2} \right)^{1/2}$$

and

$$\bar{\theta}_\Gamma := \left(\sum_{T \in \mathcal{T}_h} \sum_{e \in E(T) \cap E_h(\Gamma)} h_e \left|\left| \frac{\mathrm{d}\mathbf{g}}{\mathrm{d}\mathbf{t}_T} - \frac{\mathrm{d}\bar{\mathbf{u}}_h}{\mathrm{d}\mathbf{t}_T} \right|\right|^2_{[L^2(e)]^2} \right)^{1/2}.$$

In Table IX we show the behavior of $\hat{\theta}_\Gamma$ and $\bar{\theta}_\Gamma$ when Example 4 is solved using a uniform refinement algorithm and $\nu = 0.4900$. We observe there

that the rates of convergence for $\hat{\theta}_\Gamma$ approach 1.29 whereas for $\bar{\theta}_\Gamma$ are close to 1.5. Therefore, these boundary terms tend to zero superlinearly as h tends to zero.

Table IX: Dof, boundary terms of $\hat{\theta}$ and $\bar{\theta}$ and their experimental convergence rates (uniform refinement) (EXAMPLE 4, $\nu = 0.4900$).

$\mathcal{N}$	$\hat{\theta}_\Gamma$	$r(\hat{\theta}_\Gamma)$	$\bar{\theta}_\Gamma$	$r(\bar{\theta}_\Gamma)$
59	0.4105E+2	—	0.2430E+1	—
195	0.1770E+2	1.4070	0.8737E+0	1.7112
707	0.7834E+1	1.2658	0.3102E+0	1.6078
2691	0.3408E+1	1.2453	0.1098E+0	1.5541
10499	0.1430E+1	1.2757	0.3883E-1	1.5271
41475	0.5895E+0	1.2904	0.1373E-1	1.5135
164867	0.2415E+0	1.2930	0.4854E-2	1.5068
657411	0.9876E-1	1.2932	0.1716E-2	1.5034

In what follows, we take $\nu = 0.4900$ and consider Examples 5 and 6 to illustrate the performance of the adaptive algorithms based on $\hat{\theta}$ and $\bar{\theta}$. We remark that the solution of Example 5 has a singularity at the boundary point $(0, 0)$. In fact, the behavior of $\mathbf{u}$ in a neighborhood of the origin implies that $\mathbf{div}(\boldsymbol{\sigma}) \in [H^{1/3}(\Omega)]^2$. Thus, the expected rate of convergence for the uniform refinement is $1/3$. On the other hand, the solution of Example 6 shows large stress regions around the curve $x_1^2 + x_2^2 = 0.05^2$.

Table X: Dof, total errors, experimental convergence rates, a posteriori error estimators and efficiency indices (uniform refinement) (EXAMPLE 5).

$\mathcal{N}$	$e(\boldsymbol{\sigma}, \mathbf{u}, \boldsymbol{\gamma})$	$r(e(\boldsymbol{\sigma}, \mathbf{u}, \boldsymbol{\gamma}))$	$\hat{\theta}$	$I(\hat{\theta})$	$\bar{\theta}$	$I(\bar{\theta})$
275	0.1124E+2	—	0.1163E+2	0.9729	0.1141E+2	0.9920
1027	0.9164E+1	0.3105	0.9400E+1	0.9810	0.9279E+1	0.9939
3971	0.7320E+1	0.3323	0.7461E+1	0.9874	0.7414E+1	0.9936
15619	0.5820E+1	0.3374	0.5891E+1	0.9924	0.5875E+1	0.9952
61955	0.4622E+1	0.3374	0.4653E+1	0.9960	0.4646E+1	0.9973

In Tables X through XIII we provide the dof, the total errors, the experimental convergence rates, the values of the a posteriori error estimators $\hat{\theta}$ and $\bar{\theta}$ and the corresponding efficiency indices for the uniform and adaptive refinements as applied to Examples 5 and 6. We observe from these tables that the errors in the adaptive procedures decrease much faster than in the uniform one (see also Figures 7 and 11). In particular, we can observe in Table X that for Example 5, the experimental convergence rates for the

uniform refinement procedure approach 1/3, as predicted by the theory. In Table XI we see that the adaptive procedures based on $\hat{\theta}$ and $\bar{\theta}$ are both able to recover the linear convergence. We also observe that the efficiency indices in Example 5 are always in a neighborhood of 0.9, which confirms the reliability and eventual efficiency of the a posteriori error estimators $\hat{\theta}$ and $\bar{\theta}$.

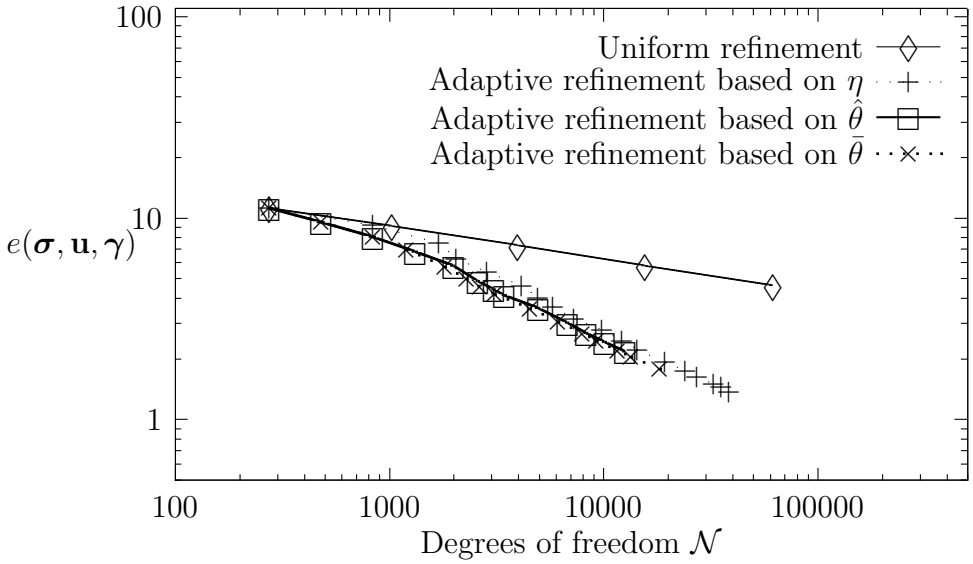

Figure 7: Total error vs. dof for the uniform and adaptive refinements (Example 5).

In Figure 7 we also display the total error versus the dof for the adaptive algorithm based on η, the a posteriori error estimator proposed in [4]. We observe that in this example the performance of the three a posteriori error estimators is quite similar. However, the efficiency indices of $\hat{\theta}$ and $\bar{\theta}$ are closer to 1 than those of η (see Figure 8).

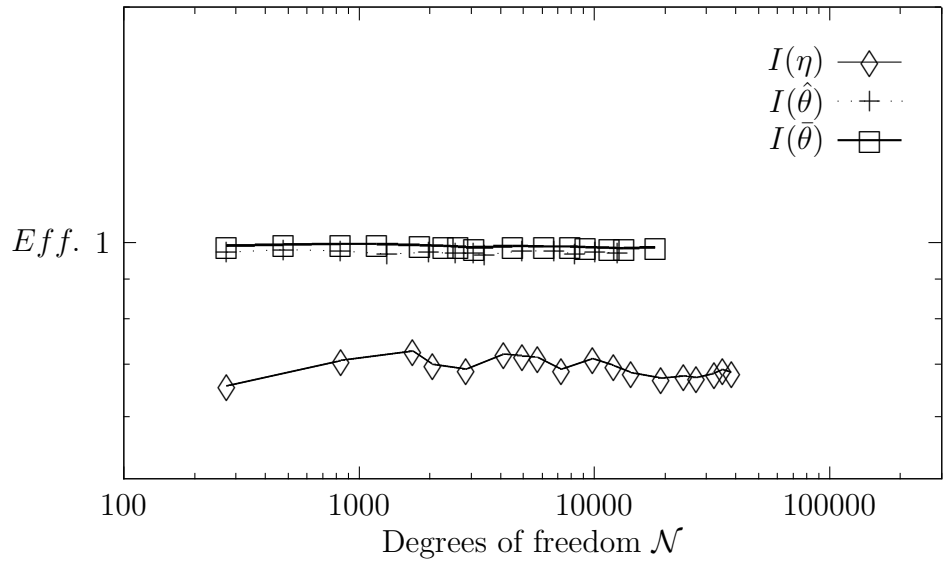

Figure 8: Efficiency indices vs. dof for adaptive refinements (EXAMPLE 5).

Table XI: Dof, total errors, experimental convergence rates, a posteriori error estimators and efficiency indices (adaptive refinement) (EXAMPLE 5).

$\mathcal{N}$	$e(\boldsymbol{\sigma},\mathbf{u},\boldsymbol{\gamma})$	$r(e(\boldsymbol{\sigma},\mathbf{u},\boldsymbol{\gamma}))$	$\hat{\theta}$	$I(\hat{\theta})$
275	0.1124E+2	—	0.1163E+2	0.9729
479	0.9518E+1	0.6065	0.9762E+1	0.9796
837	0.8073E+1	0.5904	0.8310E+1	0.9759
1323	0.6817E+1	0.7306	0.7089E+1	0.9678
1991	0.5783E+1	0.7952	0.5995E+1	0.9728
2589	0.4880E+1	1.2775	0.5089E+1	0.9689
3075	0.4439E+1	1.0772	0.4636E+1	0.9696
3433	0.4138E+1	1.2423	0.4348E+1	0.9654
4943	0.3585E+1	0.7992	0.3718E+1	0.9761
6793	0.3019E+1	1.0975	0.3122E+1	0.9763
8279	0.2688E+1	1.1538	0.2808E+1	0.9684
10145	0.2432E+1	0.9738	0.2528E+1	0.9740
12577	0.2183E+1	0.9882	0.2281E+1	0.9710
$\mathcal{N}$	$e(\boldsymbol{\sigma},\mathbf{u},\boldsymbol{\gamma})$	$r(e(\boldsymbol{\sigma},\mathbf{u},\boldsymbol{\gamma}))$	$\bar{\theta}$	$I(\bar{\theta})$
275	0.1124E+2	—	0.1141E+2	0.9920
479	0.9518E+1	0.6065	0.9607E+1	0.9954
837	0.8073E+1	0.5904	0.8137E+1	0.9967
1195	0.6982E+1	0.8124	0.7040E+1	0.9969
1815	0.5718E+1	0.9442	0.5795E+1	0.9942
2293	0.4962E+1	1.1928	0.5051E+1	0.9922
2651	0.4530E+1	1.2290	0.4628E+1	0.9906
3097	0.4181E+1	1.0038	0.4297E+1	0.9867
4511	0.3564E+1	0.8586	0.3642E+1	0.9907
6137	0.3050E+1	0.9969	0.3127E+1	0.9896
7949	0.2664E+1	1.0675	0.2726E+1	0.9889
9239	0.2449E+1	1.0951	0.2514E+1	0.9874
11613	0.2188E+1	0.9680	0.2253E+1	0.9861
13423	0.2042E+1	0.9272	0.2111E+1	0.9844
18237	0.1777E+1	0.9452	0.1818E+1	0.9887

Finally, some intermediate meshes obtained for Example 5 with the adaptive algorithms based on $\hat{\theta}$ and $\bar{\theta}$ are displayed in Figures 9 and 10, respectively. We remark that both algorithms are able to localize the singularity of the solution, although refinements appear to be slightly more localized when using $\bar{\theta}$.

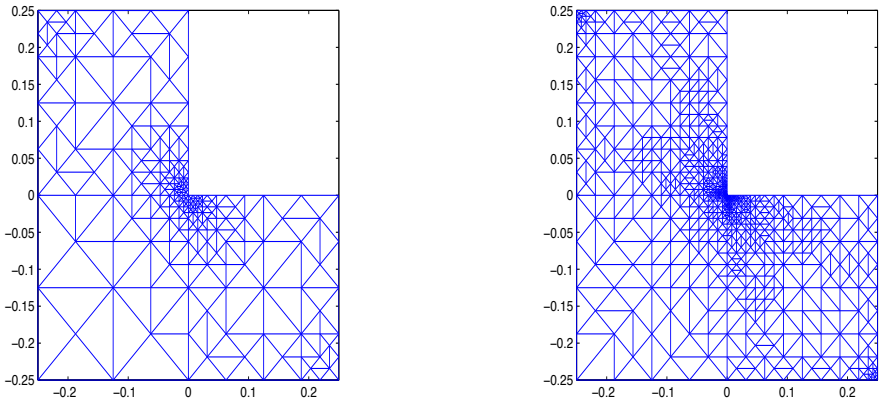

Figure 9: Adapted meshes obtained using $\hat{\theta}$ in EXAMPLE 5
1991 dof (left) and 8279 dof (right)

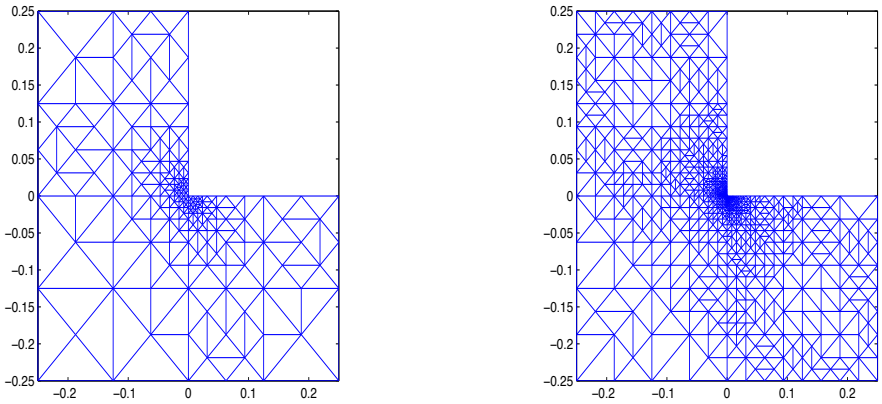

Figure 10: Adapted meshes obtained using $\bar{\theta}$ in EXAMPLE 5
1815 dof (left) and 9239 dof (right)

For Example 6, the convergence of the adaptive algorithms based on $\hat{\theta}$ and $\bar{\theta}$ is much faster that that of the uniform refinement procedure, as can be seen from Tables XII and XIII, and from Figure 11. We can observe in Figure 11 that the performance of the three a posteriori error estimators available for this problem is quite similar. We also observe in Tables XII and XIII that the efficiency indices in Example 6 are always in a neighborhood of 0.9, which confirms the reliability and eventual efficiency of the a posteriori error

estimators $\hat{\theta}$ and $\bar{\theta}$. In Figure 12, we display the efficiency indices of $\hat{\theta}$, $\bar{\theta}$ and η, and we observe that, again, the efficiency indices of $\hat{\theta}$ and $\bar{\theta}$ are closer to 1 than those of η.

Table XII: Dof, total errors, experimental convergence rates, a posteriori error estimators and efficiency indices (uniform refinement) (EXAMPLE 6).

$\mathcal{N}$	$e(\boldsymbol{\sigma}, \mathbf{u}, \boldsymbol{\gamma})$	$r(e(\boldsymbol{\sigma}, \mathbf{u}, \boldsymbol{\gamma}))$	$\hat{\theta}$	$I(\hat{\theta})$	$\bar{\theta}$	$I(\bar{\theta})$
1407	0.7722E+1	—	0.7836E+1	0.9871	0.7750E+1	0.9980
5451	0.4709E+1	0.7281	0.4829E+1	0.9784	0.4741E+1	0.9965
21459	0.2597E+1	0.8643	0.2714E+1	0.9629	0.2631E+1	0.9933
85155	0.1344E+1	0.9496	0.1426E+1	0.9524	0.1374E+1	0.9887

Table XIII: Dof, total errors, experimental convergence rates, a posteriori error estimators and efficiency indices (adaptive refinement) (EXAMPLE 6).

$\mathcal{N}$	$e(\boldsymbol{\sigma}, \mathbf{u}, \boldsymbol{\gamma})$	$r(e(\boldsymbol{\sigma}, \mathbf{u}, \boldsymbol{\gamma}))$	$\hat{\theta}$	$I(\hat{\theta})$
1407	0.7722E+1	—	0.7836E+1	0.9871
1619	0.4710E+1	7.0286	0.4814E+1	0.9811
2119	0.2631E+1	4.3256	0.2704E+1	0.9761
2985	0.1526E+1	3.1778	0.1567E+1	0.9771
7379	0.7903E+0	1.4459	0.8279E+0	0.9613
21910	0.4241E+0	1.1371	0.4463E+0	0.9604
49644	0.2834E+0	0.9874	0.2951E+0	0.9702
$\mathcal{N}$	$e(\boldsymbol{\sigma}, \mathbf{u}, \boldsymbol{\gamma})$	$r(e(\boldsymbol{\sigma}, \mathbf{u}, \boldsymbol{\gamma}))$	$\bar{\theta}$	$I(\bar{\theta})$
1407	0.7722E+1	—	0.7750E+1	0.9980
1619	0.4710E+1	7.0286	0.4737E+1	0.9972
2119	0.2631E+1	4.3256	0.2647E+1	0.9969
3015	0.1523E+1	3.0980	0.1534E+1	0.9960
7679	0.7825E+0	1.4166	0.7945E+0	0.9920
24156	0.4066E+0	1.1348	0.4167E+0	0.9872
87322	0.2078E+0	1.0347	0.2157E+0	0.9809

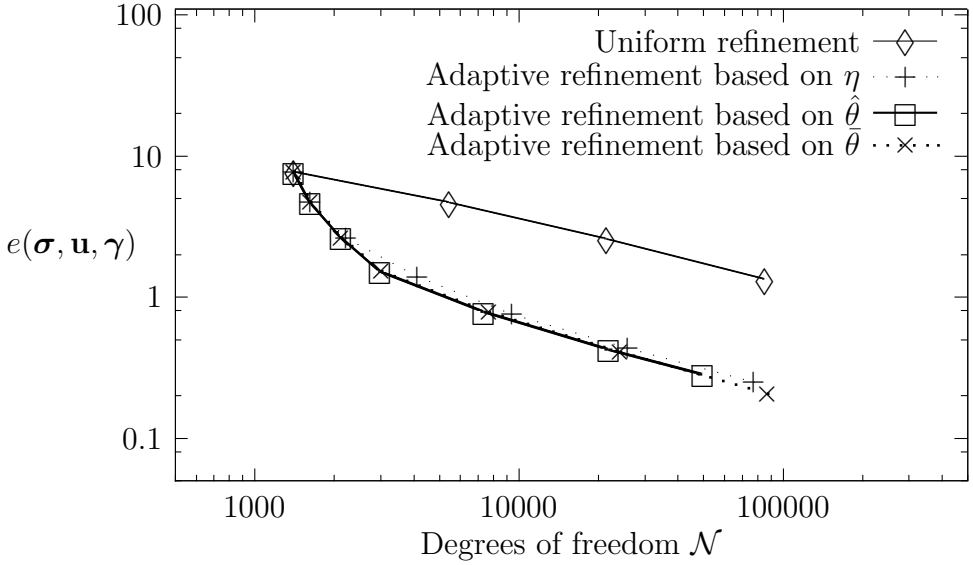

Figure 11: Total error vs. dof for the uniform and adaptive refinements (EXAMPLE 6).

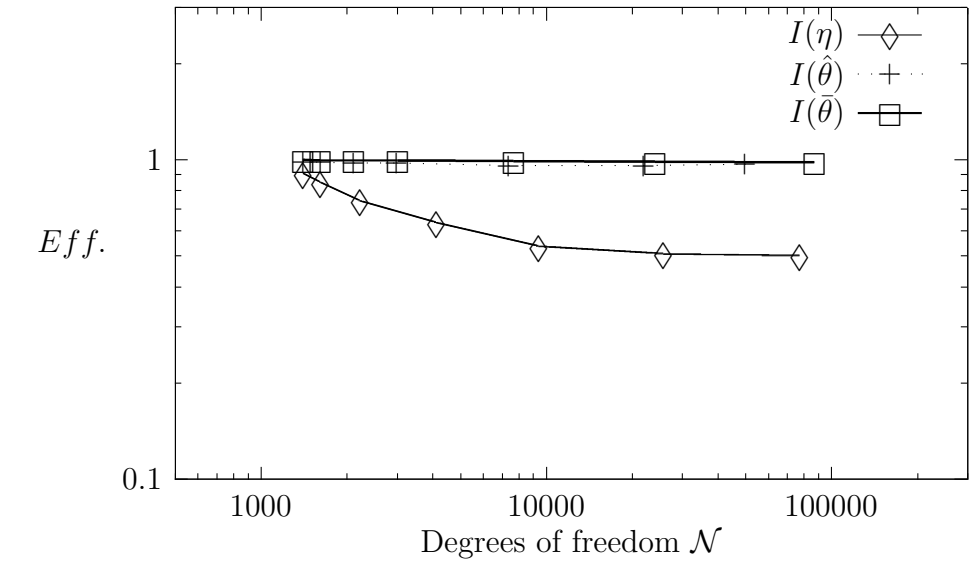

Figure 12: Efficiency indices vs dof for adaptive refinements (EXAMPLE 6).

Finally, some intermediates meshes obtained with the adaptive algorithms based on $\hat{\theta}$ and $\bar{\theta}$ are displayed in Figures 13 and 14, respectively. We re-

mark that both algorithms are able to localize the large stress regions of the solution. In this case, there are practically no visible differences between the meshes obtained with $\hat{\theta}$ and $\bar{\theta}$.

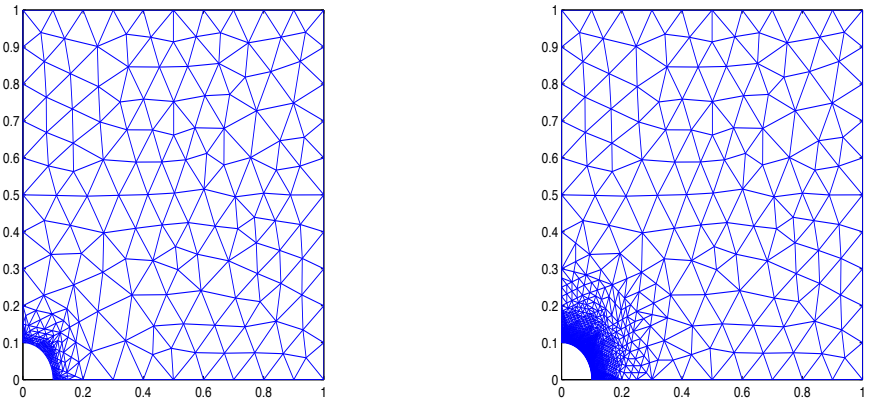

Figure 13: Adapted meshes obtained using $\hat{\theta}$ in EXAMPLE 6
2985 dof (left) and 21910 dof (right)

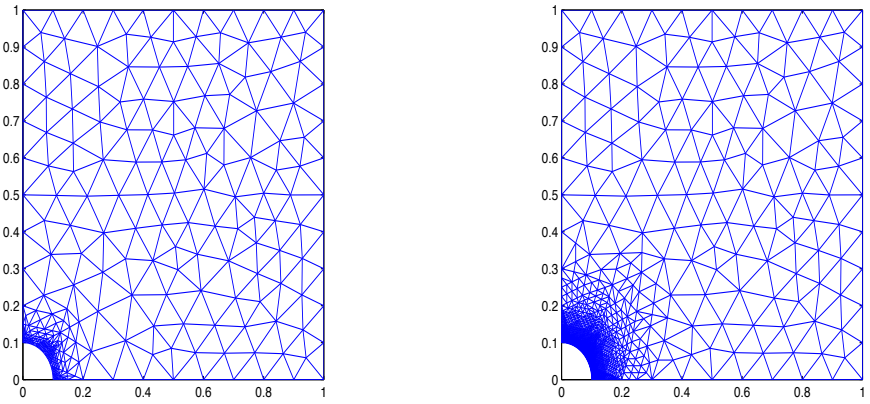

Figure 14: Adapted meshes obtained using $\bar{\theta}$ in EXAMPLE 6
3015 dof (left) and 24156 dof (right)

5. Conclusions

We obtained new a posteriori error estimators for the augmented dual-mixed finite element methods introduced in [11]-[13] for the linear elasticity

system with Dirichlet boundary conditions. One special feature of the new estimators is that they do not involve normal nor tangential jumps, being much simpler than the a posteriori error estimators available in the literature (cf. [3, 4]).

In the case of pure homogeneous Dirichlet boundary conditions, the new a posteriori error estimator is reliable, locally efficient and only requires the computation of four residuals per element. Moreover, it can be used in two- and three-dimensional problems and with any finite element subspaces. In the case of non-homogeneous Dirichlet boundary conditions, we derived two reliable a posteriori error estimators, $\hat{\theta}$ and $\bar{\theta}$. The a posteriori error estimator $\hat{\theta}$ can be used in two and three dimensions and with any finite element subspaces, whereas the a posteriori error estimator $\bar{\theta}$ was derived for two-dimensional problems assuming a piecewise linear discretization of the displacement. Moreover, $\bar{\theta}$ is locally efficient over the elements that do not touch the boundary.

Numerical experiments support the theoretical results. In all the experiments, the adaptive algorithms converge faster than the corresponding uniform procedure and are able to localize the singularities and large stress regions of the solutions. Numerical comparisons with the a posteriori error estimators proposed in [3, 4] support the use of the new a posteriori error estimators in practice.

Acknowledgments. This research has been partially supported by Universidade da Coruña. The research of the first and second authors is partially supported by CONICYT-Chile through FONDECYT Grants 11060014 and 11070085, and by Dirección de Investigación of Universidad Católica de la Santísima Concepción. The research of the third author is supported by MICINN project MTM2010-21135-C02-01.

References

[1] D.N. Arnold and W.L. Wendland. On the Asymptotic Convergence of Collocation Methods. Math. Comp. 41, 349–381 (1983).

[2] T.P. Barrios and G.N. Gatica. An augmented mixed finite element method with Lagrange multipliers: A priori and a posteriori error analyses. J. Comput. Appl. Math. 200, 653–676 (2007).

[3] T.P. Barrios, G.N. Gatica, M. González and N. Heuer. A residual based a posteriori error estimator for an augmented mixed finite element method in linear elasticity. M2AN Math. Model. Numer. Anal. 40, 843–869 (2006).

[4] T.P. Barrios, E.M. Behrens and M. González. A posteriori error analysis of an augmented mixed formulation in linear elasticity with mixed and Dirichlet boundary conditions. Comput. Methods Appl. Mech. Engrg. 200, 101-113 (2011).

[5] D. Braess, O. Klaas, R. Niekamp, E. Stein and F. Wobschal. Error indicators for mixed finite elements in 2-dimensional linear elasticity. Comput. Methods Appl. Mech. Engrg. 127, 345-356 (1995).

[6] C. Carstensen. An a posteriori error estimate for a first-kind integral equation. Math. Comp. 66 (217), 139-155 (1997).

[7] C. Carstensen, P. Causin and R. Sacco. A posteriori dual-mixed adaptive finite element error control for Lamé and Stokes equations. Numer. Math. 101, 309-332 (2005).

[8] C. Carstensen and G. Dolzmann. A posteriori error estimates for mixed FEM in elasticity. Numer. Math. 81, 187-209 (1998).

[9] C. Carstensen, G. Dolzmann, S.A. Funken and D.S. Helm. Locking-free adaptive mixed finite element methods in linear elasticity. Comput. Methods Appl. Mech. Engrg. 190, 1701-1718 (2000).

[10] W. Dahmen, B. Faermann, I.G. Graham, W. Hackbusch and S.A. Sauter. Inverse inequalities on non-quasi-uniform meshes and application to the Mortar element method. Math. Comp. 73, 1107–1138 (2003).

[11] G.N. Gatica. Analysis of a new augmented mixed finite element method for linear elasticity allowing $\mathbb{RT}_0$-$\mathbb{P}_1$-$\mathbb{P}_0$ approximations. M2AN Math. Model. Numer. Anal. 40, 1–28 (2006).

[12] G.N. Gatica. An augmented mixed finite element method for linear elasticity with non-homogeneous Dirichlet conditions. Electronic Transactions on Numerical Analysis 26, 421-438 (2007).

[13] G.N. Gatica, A. Márquez and S. Meddahi. An augmented mixed finite element method for 3D linear elasticity problems. J. Comput. Appl. Math. 231 (2), 526-540 (2009).

[14] R. Hiptmair. Finite elements in computational electromagnetism. Acta Numerica, pp. 237–339 (2002).

[15] M. Longsing and R. Verfürth. A posteriori error estimators for mixed finite element methods in linear elasticity. Numer. Math. 97, 757-778 (2004).

[16] R. Verfürth. A review of a posteriori error estimation techniques for elasticity problems. Comput. Methods Appl. Mech. Engrg. 176, 419-440 (1999).